Deep Space CubeSat Constellation System

a project presented to
The Faculty of the Department of Aerospace Engineering
San José State University

in partial fulfillment of the requirements for the degree
Master of Science in Aerospace Engineering

by

Subhiksha Raman

May 2021

approved by

Dr. Periklis Papadopoulos
Faculty Advisor

ABSTRACT

Deep Space CubeSat Constellation System

Subhiksha Raman

CubeSats provide a low-cost alternative to static landers and mobile platforms in deep space, which allows for greater launch accessibility and scientific return. Their use in constellation systems allows for complete coverage over a planet or moon, which helps to reduce costs while performing large-scale research for supporting missions. This report shows the design process of a sample deep space CubeSat constellation system, starting with developing subsystem requirements and constraints using existing data from other constellations. Results of design optimization and simulations are shown using set design parameters. Calculations performed in this report can be replicated for other deep space CubeSat constellation designs.

ACKNOWLEDGMENTS

I would first like to thank Dr. Periklis Papadopoulos for helping me develop the final idea for this project, as well as being available to answer my questions throughout the process. I also extend my gratitude to Dr. Nikos Mourtos and the rest of the Aerospace Engineering department at SJSU for providing me with and helping me hone the skills needed for this project and in my future career.

Finally, I thank my parents, my grandparents, and the rest of my family for their support in my past, present, and future endeavors.

TABLE OF CONTENTS

LIST OF TABLES

LIST OF FIGURES

LIST OF SYMBOLS

Symbol	Definition	Given Values, if any	Units
Power Subsystem			
P_e	Spacecraft's power requirement during eclipse		W
P_d	Spacecraft's power requirement during daylight		W
T_e	Period length of eclipse orbit		s
T_d	Period length of daylight orbit		s
X_e	Transmission efficiency during eclipse		
X_d	Transmission efficiency during daylight		
P_{sa}	Power needed from solar array during daylight		W
P_O	Ideal solar cell performance		W/m^2
I_d	Inherent degradation	0.77	
θ	Sun incidence angle	23.5 (worst case), 90 (max power)	Degrees
P_{BOL}	Beginning-of-life power per unit area		W/m^2
L_d	Life degradation of solar array		
P_{EOL}	End-of-life power per unit area		W/m^2
τ_e	Eclipse duration		s
DOD	Depth of discharge	0.20-0.80	
N	Number of batteries		
n	Transmission efficiency of the battery		
C_r	Required battery capacity		W-hr
Communications Subsystem			
DR	Data rate		bps
F	Fractional reduction in viewing time		
T_{max}	Maximum time in view		s
$T_{initiate}$	Time required to initiate comms pass		s
M	Margin needed to account for missed passes	2-3	
DQ	Quantity of data		bits
P	Transmitter power		dBW
L_l	Transmitter-to-antenna line loss		dB
G_t	Transmit antenna gain		dBi
L_s	Space loss		dB
c	Speed of light	3.00×10^8	m/s
S	Path length		
f	Frequency		GHz

L_a	Transmission path loss	-0.3	dB
L_θ	Antenna pointing loss		dB
e	Pointing error		
θ	Antenna half-power beamwidth		degrees
D	Antenna diameter		m
G_r	Receive antenna gain		dBi
k	Boltzmann's constant	1.38×10^{-23}	J/K
T_s	System noise temperature		K
E_b/N_o	Ratio of received energy-per-bit to noise density	50-100	dB
W_f	Power flux density		dBW/m^2
GN&C Subsystem			
T_D	Worst-case disturbance torque		N-m
MF	Margin Factor		
T_{RW}	Reaction-wheel torque due to disturbance rejection		N-m
T_G	Maximum gravity torque		N-m
T_{sp}	Solar radiation torque		N-m
T_m	Magnetic torque		N-m
T_a	Aerodynamic torque		N-m
θ	Slewing angle	30	degrees
I	Moment of inertia		m^4
t	Minimum maneuver time		s
T_{slew}	Slew torque		N-m
τ	Orbit period		s
h	Wheel momentum		N-m-s
Propulsion Subsystem			
I_{sp}	Specific impulse	50-75	s
F	Thrust	0.05-200	N
$\dot{m}$	Propellant mass flow rate		kg/s
V_e	Propellant exhaust velocity		m/s
A_e	Nozzle exit area		m^2
g	Acceleration due to gravity	9.81	m/s^2
γ	Specific heat ratio for gas		
R_A	Universal gas constant	8.314	J/K-mol
MW	Molecular weight of gas		
T_c	Chamber temperature		K
P_e	Gas pressure at nozzle exit		Pa
P_c	Chamber pressure		Pa
A_t	Nozzle throat area		m^2

ε	Area expansion ratio		
c^*	Characteristic velocity		m/s
c_f	Thrust coefficient		
Structures Subsystem			
E	Young's Modulus	71×10^9	N/m^2
ν	Poisson's Ratio	0.33	
ρ	Density	2.8×10^3	kg/m^3
F_{tu}	Ultimate tensile strength	524×10^8	N/m^2
F_{ty}	Yield tensile strength	448×10^6	N/m^2
A	Cross-sectional area		m^2
m_B	Estimated distributed mass		kg
L	Length		m
I	Area moment of inertia		m^4
b	Base length of cross-section		m
H	Height of cross-section		m
f_{nata}	Axial frequency		Hz
f_{natl}	Lateral frequency		Hz
LF	Loading factor		
M	Bending moment		N-m
P_{eq}	Equivalent axial load		N
y	Moment arm		m
FS	Factor of safety	1.25 (ultimate), 1.1 (yield)	
P_{cr}	Critical buckling load		N
MS	Margin of safety		
m_{box}	Mass of CubeSat box		kg
~~V~~	Volume		m^3
P	Maximum expected operating pressure		Pa
r	Radius		m
t	Thickness		m
σ	Allowable stress		N/m^2
A_{sa}	Area of solar array		m^2
m_a	Mass of solar arrays		kg
g	Acceleration due to gravity	9.81	m/s^2
Payload Subsystem			
Z_C	Number of cross-track pixels		
Z_A	Number of swaths in one second		swath/s
B	Number of bits per pixel		
DR	Data rate		bps
η	Maximum sensor look angle		degrees

IFOV	Instantaneous field of view		
V_g	Spacecraft ground-track velocity		m/s
H	Orbit altitude		km
Y_{max}	Maximum along-track ground sampling distance		m
Rs	Slant range		m
N_m	Number of pixels on instrument scanner		
τ_i	Pixel integration period		s
λ	Operating wavelength		m
F	Focal length		m
Q	Quality factor for imaging		
d	Width for square detectors		m
R	Aperture ratio, new to old		
K	Aperture factor	2 (if R < 0.5), 1 (otherwise)	
Orbital Mechanics			
$\mathbf{p_Q}$	General perturbation force vector		N
F	Thrust	0.05-200	N
$\mathbf{v_Q}$	Velocity vector		km/s
$\mathbf{p_{thrust}}$	Thrust perturbation vector		N
ρ	Density of atmosphere		kg/m^3
$v_{satellite}$	Velocity of satellite		km/s
C_D	Coefficient of drag		
A	Cross-sectional area		m^2
p_{drag}	Drag scalar of satellite		N
R	Reflection factor	0 (absorption), 1 (specular reflection), 0.4 (diffuse reflection)	
$p_{radiation}$	Solar radiation perturbation		N
a	Length of semi-major axis		km
e	Eccentricity		
i	Inclination		degrees
Ω	Right ascension of ascending node		degrees
G	Gravitational constant	6.67×10^{-20}	$km^3/kg\text{-}s^2$
M	Mass of planet or moon		kg
τ	Orbit period		s
h	Angular momentum		km^2/s
h	Angular momentum vector		km^2/s
n	Magnitude of Line of Nodes		km^2/s
n	Line of Nodes		km^2/s

λ_{street}	Street of coverage angle		degrees
λ_{max}	Maximum central angle		degrees
D_{max}	Maximum perpendicular separation between two adjacent planes		degrees
S	Space between satellites in each plane		degrees
N_p	Number of satellites per plane		
t_{rev}	Revisit time		s
l^{E-P}	Rotational matrix		

1. INTRODUCTION

The following chapter will focus on the motivation for developing CubeSat constellation systems and its use for deep space missions. A summary of the literature review will provide additional information on CubeSats and general constellation systems, as well as their subsystems. Both the motivation and literature review shape the main objective of this project and methodology used.

1.1 MOTIVATION

Until recently, two types of spacecraft have been considered for deep space missions: static landers and mobile platforms. Now nanosatellite technology, especially CubeSats, provide a low-cost alternative through greater launch accessibility and scientific return. The ability to carry small instruments through multiple small, disposable spacecraft, as well as access to a variety of terrains, make CubeSats ideal for such missions [1].

The same applies for CubeSat constellation systems, as well as the need for zonal or global coverage of a body such as the Earth. Traditional constellation design methods incorporate continuous or discontinuous coverage of a specific geographic region [2]. Usually, the objectives behind using these systems include providing connectivity across a specific region or performing large-scale scientific research in weather patterns.

Though Earth-orbiting constellation systems are becoming more common, there are currently no existing deep space constellation systems. However, deep space nanosatellites are currently in development and are capable of performing such high-risk and high-science return missions [1]. These missions can include communicating with rovers or other larger spacecraft on other planets or moons. However, these types of missions still do not cover as much area over a planet or moon due to the various spacecraft constraints such as size or speed.

Using CubeSat constellation systems in deep space missions can help cover larger regions of planets or moons. One CubeSat would act as a mother ship, while the others would act as daughter ships and cover different areas around the planet or moon [3]. The more satellites used in the system, the more the propellent mass in each satellite can be reduced, thus reducing the cost-to-orbit [4].

1.2 LITERATURE REVIEW

This section will cover information on small satellites, including CubeSats, and their deep space missions. Additionally, it will cover various types of constellation systems and their respective missions.

1.2.1 Small Satellites Overview

Small satellites (smallsats) in general are classified as satellites with mass less than 180 kg, or the size of a large kitchen fridge. Table 1.1 shows the five main classes of smallsats [5]:

Table 1.1: Classes of small satellites.

Class	**Mass (kg)**
Minisatellite	100 – 180
Microsatellite	10 – 100
Nanosatellite	1 – 10
Picosatellite	0.01 – 1

Femtosatellite	0.001 – 0.01

One example of a smallsat mission is Janus SIMPLEx, a Lockheed Martin mission which will use a dual small deep space spacecraft system to visit near-earth binary asteroids [6]. The system consists of ESPA-class, dual small satellites weighing around 40 kg each. The satellites will also carry visible and infrared cameras to take pictures of the system. One key mission requirement is to meet the planetary launch window, since it is a deep space mission. Some subsystem requirements for the satellites used are that their power systems must handle a range of Sun distances and that their telecommunications systems need to be able to transmit over long distances and be compatible with the Deep Space Network [6].

Nanosatellites are used for extremely low-cost missions and can be used to support larger missions to increase science return. Rather than using static landers or mobile platforms, they allow for an alternative approach for in-situ and close proximity observations in a variety of terrains through a distribution of multiple small, disposable spacecraft across the surface. Until recently, they were only used in low-Earth orbit missions but can be used as instruments part of larger missions, particularly as interplanetary CubeSats [1].

1.2.1.1 CubeSats Overview

CubeSats, a class of nanosatellites with a standard size and form factor, are especially popular because their fixed design makes launching easier and allows for a viable market for common components. They also have a low cost of entry into development and a low-cost of failure. One standard form factor is 1U, or a 10 x 10 x 10 cm cube, and each 1U of volume weighs 1 or 2 kg. Table 1.2 shows the most common factors along with their mass, volume (before deployment), and power parameters [1,7]:

Table 1.2: Common form factors for CubeSats.

Standard Form Factor	**Mass (kg)**	**Volume (cm^3)**	**Power, fixed (W)**	**Power, deployed (W)**
1U	1.5	10x10x10	~3	-
3U	4.5	10x10x30	~8	~25
6U	10	10x20x30	~14	~35

Typical CubeSat characteristics include low mass or inertia and low risk to the primary spacecraft. By using them as instruments themselves, CubeSats can support science experiments, such as imaging and remote sensing and direct surface sampling, and they are often driven by science applications. Because of these characteristics, they can enable both alternatives and augmentations to larger missions to low Earth orbit, geostationary orbit, and deep space.

Other parameters for CubeSat design include the following [1]:

- Solar Arrays (fixed and/or deployable)
- Battery
- Antenna (monopole/dipole, turnstile, patch, 1U dish)
- Communications (UHF/VHF, S-Band)
- Data Rates
- Attitude Control (passive, torquer, drag control, etc.)

- Command & Data Handling (software)
- Propulsion
- Deployable Instruments (antenna, panels, tethers, boom, solar sail)
- Demonstrated Lifetime
- Payload Instruments (camera, telescopes, etc.)

The parameters listed above depend on the size of the CubeSat. For example, a 1U CubeSat does not have a propulsion system, but a 3U or 6U CubeSat has a cold gas thruster, electric propulsion, and solar sail [1]. If the CubeSat is larger, then it has greater performance and can hold more instruments in its payload. A larger CubeSat can also carry a higher-powered battery and antenna.

However, the risk and main drawback of using CubeSats is that there is still low technological readiness level (TRL) in deep space [1,8]. Key technological developments are being made to support interplanetary missions, such as radiation-tolerant operation strategies, deep-space deployment, and nanosat surface mobility.

1.2.1.2 Deep Space CubeSat Mission Example

The NASA probe InSight traveled with two briefcase-sized CubeSats, together called Mars Cube One (MarCO), in 2018. These CubeSats, each with a mass of 13.5 kg, represented the first mission to test CubeSats in deep space. The purpose of MarCO was to serve as communications relays during InSight's landing and to send data from the probe to the Mars Reconnaissance orbiter [9]. To do so, the CubeSats carried two main scientific instruments: UHF Radio Receiver and X Band Radio Transmitter. Additionally, the CubeSats used a "reflectarray," a flat antenna patterned to mimic a parabolic dish to help focus transmissions towards Earth [9,10].

As of 2019, the mission team lost contact with the MarCOs possibly due to attitude-control issues causing the CubeSats to wobble and lose their ability to send and receive commands. Other possible factors include malfunctions in its thruster or brightness sensors. Still, they consider the mission a success. Critical spare parts (i.e. experimental radios, antennas, and propulsion systems) will be used in future deep space CubeSat missions [10].

1.2.2 Constellation Systems Overview

Satellite constellation systems are predominantly used for communication, navigation, and remote sensing applications [2]. Communication and navigation applications include Internet connectivity services and Global Positioning Systems (GPS), respectively. Remote sensing applications include research-quality science in systems such as the following:

- Space Technology 5 (ST5) Project
- the NASA Time-Resolved Observations of Precipitation Structure and Storm Intensity with a Constellation of Smallsats (TROPICS) mission
- NASA Hyperspectral CubeSat Constellation

These systems are ideal for objectives that require coverage for a large geographic region, since they consist of more than one satellites working together as a system. Of the three listed above, ST5 and TROPICS are actual missions; as of 2015, the hyperspectral CubeSat constellation is still a concept presented by NASA scientists at a conference.

1.2.2.1 ST5 Project Overview

The ST5 Project, launched in March of 2006 and decommissioned after 90 days, was a constellation of three microsatellites in a "string of pearls" orientation. Each spacecraft was around

25 kg in mass and 53 cm in diameter by 48 cm in height, and included the subsystems and components shown in Figure 1.1 below [11]:

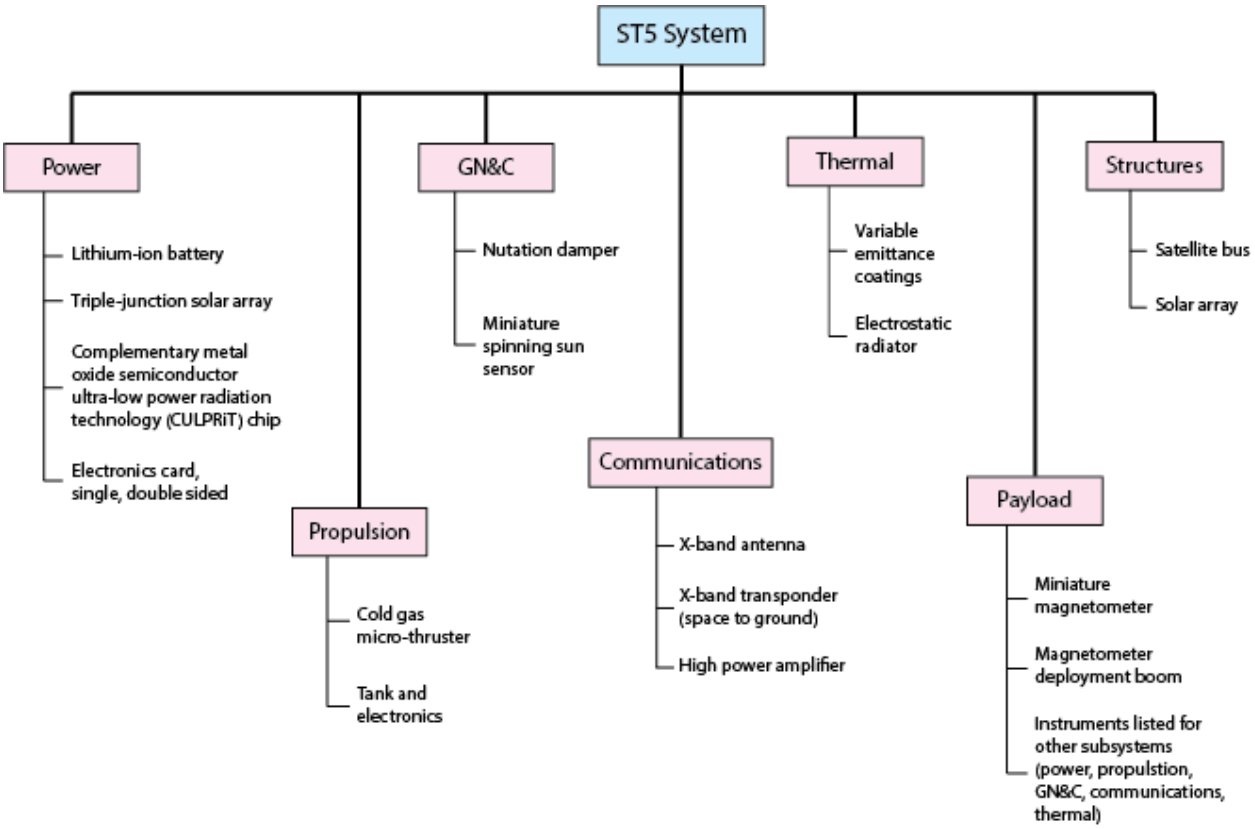

Figure 1.1 – System decomposition of ST5 Project.

Several components, such as the nutation damper from the guidance, navigation, and control (GN&C) subsystem and cold gas micro-thruster from the propulsion subsystem, are connected to those in other subsystems through interdisciplinary coupling. For example, both the nutation damper and cold gas micro-thruster are used for transportation purposes. The power subsystem, which operates under low voltage, is responsible for powering all of the components and other subsystems in each of the satellites; therefore, it is the most important subsystem in this constellation system [11].

The objective of the ST5 mission was to show that a constellation of microsatellites was capable of performing research-quality science. In this case, the spacecraft observed changes in the Earth's magnetic field, and in doing so, it met its objective. Instruments such as the battery, magnetometer, and ground system components were used in future missions.

1.2.2.2 NASA TROPICS Overview

The NASA TROPICS mission is a constellation system of six 3U CubeSats[1] in three different low-Earth orbital planes [12]. Each CubeSat included the subsystems and components shown in Figure 1.2 below [13]:

[1] See Section 1.2.1 for more information on size of CubeSats

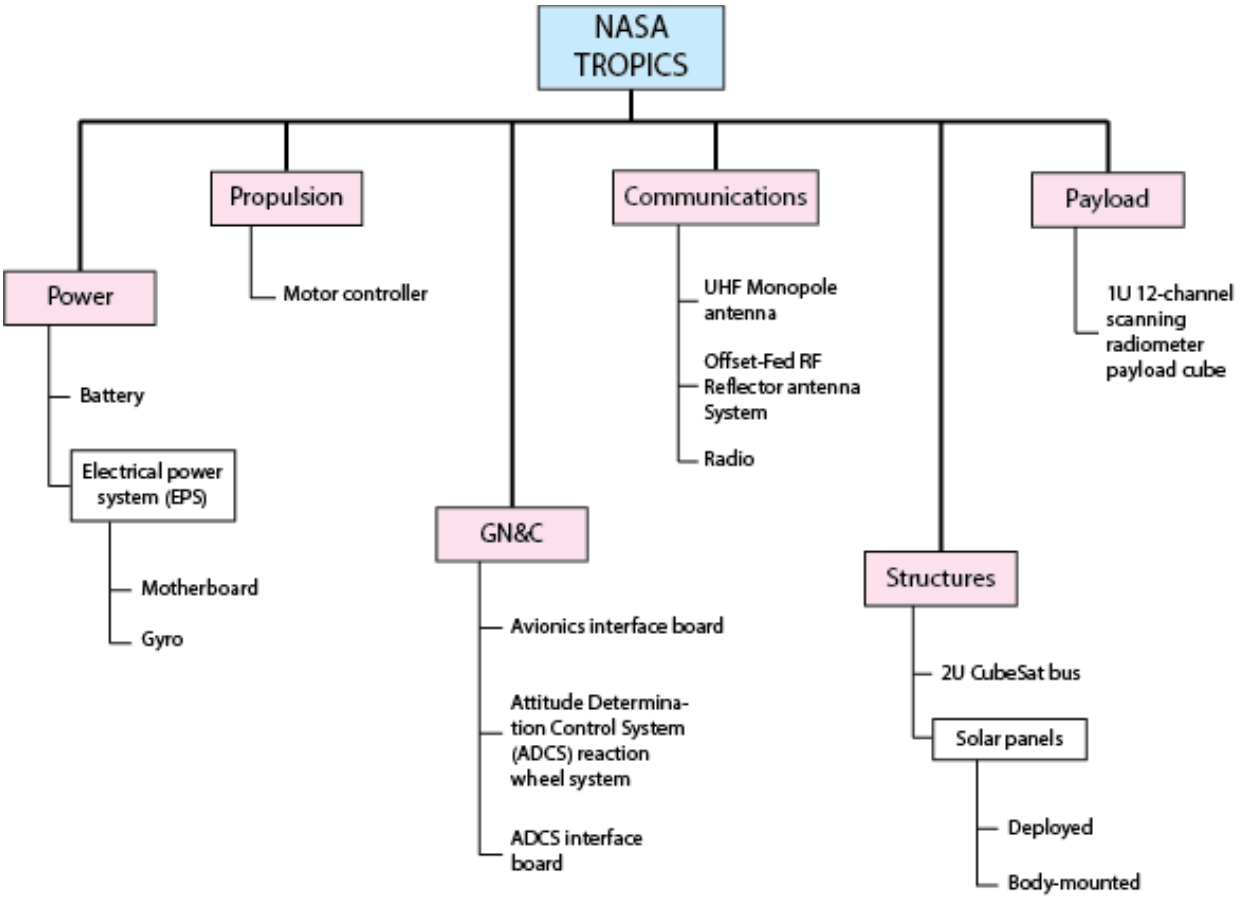

Figure 1.2 – System decomposition of NASA TROPICS mission.

Similar to the ST5 mission, several components in the TROPICS mission are connected to those in other systems. The CubeSat bus houses all of the other components within the unit, save for the solar panels. The motor controller and the instruments used for the GN&C subsystem help guide each CubeSat to gather data over a specific area using the radiometer payload cube [12]. Therefore, in this case, the most important subsystem in this constellation system is the GN&C subsystem.

The main goal of the TROPICS mission is to provide weather observations of 3D atmospheric temperature and humidity, cloud ice and precipitation horizontal structure, and storm intensity [12]. These observations will help analyze relationships between the different types of data and various weather patterns to provide more insight into storm processes such as hurricanes [13]. Currently, the mission is under development and will be launched sometime in the near future.

1.2.2.3 NASA Hyperspectral CubeSat Constellation Overview

The main goal for a hyperspectral CubeSat constellation is to provide daily or diurnal coverage at any point on the Earth cost-effectively [14]. This concept was developed by team members of the Earth Observing 1 (EO-1) mission, which carried an imaging spectrometer to capture images of natural hazards for more than 15 years. Eventually, they needed a way to take the images on a daily basis, which proved impossible using EO-1.

The constellation system has two possible configurations. The first one would contain three CubeSats at one time, angled at 30 degrees each. These would then be replaced at a set time, either all at once annually or one by one every four months. The other configuration would have 15

CubeSats, which helps in observing select spots on Earth every 46 minutes. The constellation would require three sets of the 15 CubeSats to be able to select any spot on the Earth. Each CubeSat would include the subsystems and off-the-shelf components shown in Figure 1.3 below [14]:

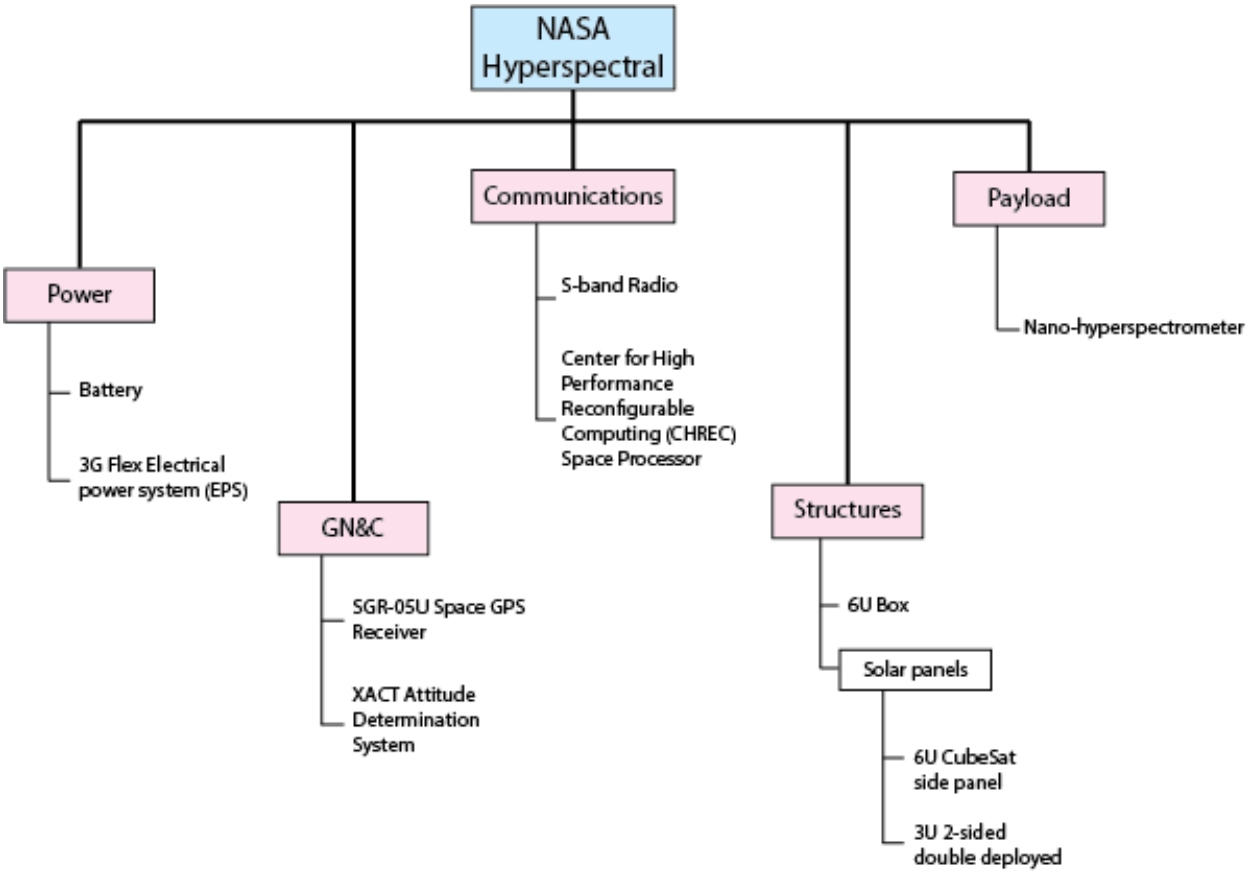

Figure 1.3 – System decomposition of NASA hyperspectral mission.

The CubeSat system presented in Figure 1.3 is similar to the two shown in Figure 1.1 and Figure 1.2. All three contain a battery and EPS as part of its power subsystem, and all three have similar structural components (bus/box and solar panels). The performance of the nano-hyperspectrometer depends on the location of the CubeSats and data relay. Therefore, the two most important subsystems in this concept are communications and GN&C.

Components for the propulsion subsystem were not included in the conceptual design. However, based on information presented in section 1.2.1.1, each CubeSat could be able to have a cold gas thruster due to its 6U size.

1.2.2.4 Constellation System Design and Coverage

As mentioned in section 1.1, there are two main types of constellation design methods: continuous and discontinuous global coverage. Both methods have both simple and complex designs. To design a constellation system, the following assumptions are made [2]:

1. The Earth is considered a round body.
2. All satellites in a constellation will be at the same altitude with the same number of satellites in each orbit plane.
3. All orbit planes in a constellation will have the same orbit inclination.

In simple continuous global coverage, at least one satellite is visible above a minimum elevation angle at every point on the Earth's surface. Complex continuous coverage can either be full or partial region coverage, useful for telecommunications and navigation purposes. Theoretical designs such as the Draim or Walker constellations can achieve ideal continuous global coverage, which use four satellites and circular orbits, respectively [2,4]. The Draim constellation design, in particular, can incorporate perturbations only if there is a common period and similar inclination between the satellites.

On the other hand, simple discontinuous coverage implies that every point on the surface is viewed with a predefined revisit time, which ranges from a few minutes to a few hours. Similarly, complex discontinuous coverage can either be full or partial region coverage with revisit times. These types of constellation systems have become more prevalent only within the last decade, but they have proved to be especially useful for remote sensing applications or weather observations [2,15].

1.3 PROJECT PROPOSAL

The objective of this project is to develop a constellation of CubeSats to augment a deep space mission, such as a mission to the outer solar system.

1.4 METHODOLOGY

The methodology of this project is as follows:

- Determine mission and subsystem requirements based on literature review presented in section 1.2, analysis, and interdisciplinary coupling between subsystems
- Develop high level designs of the top five subsystems based on the requirements already determined
- Perform design of experiments to identify key parameters and performance drivers
- Develop simulations of the constellation system

2. DESIGN OF CUBESAT SUBSYSTEMS

The following chapter will use the information gathered in the literature review presented earlier (see Section 1.2) to design each CubeSat in the constellation system for this project. This will comprise high-level designs for each subsystem, including inputs and outputs for relevant equations as well as design variables and constants.

2.1 SUBSYSTEMS OVERVIEW

Based on the system decompositions of the three missions presented in Section 1.2.2, the common subsystems are as follows:

- Power
- Communications
- GN&C
- Structures
- Payload

Therefore, a deep space CubeSat constellation should include the subsystems listed above. Coincidentally, those subsystems are all of the ones listed for the two CubeSat constellation systems; the ST5 system also contained the propulsion and thermal subsystems. Table 2.1 shows the different components for each subsystem in each CubeSat constellation presented earlier:

Table 2.1: Comparison of subsystems in different CubeSat constellations.

	Constellation System Components		
Subsystem	**ST5 System**	**NASA Tropics**	**NASA Hyperspectral**
Power	Battery	Battery	Battery
	Solar array		
	CULPRiT chip	EPS (not including battery)	EPS (not including battery)
	Electronics card		
Communications	X-band antenna	UHF monopole antenna	S-band radio
	X-band transponder	RF reflector antenna system	CHREC space processor
	Amplifer	Radio	
GN&C	Nutation damper	Avionics interface board	GPS receiver
	Mini sun spinning sensor	ADCS reaction wheel system	Attitude determination system
		ADCS interface board	
Structures	Satellite bus	2U bus	6U box
	Solar array	Solar panels	Solar panels
Payload	Mini magnetometer	Radiometer payload cube	Nano-hyperspectrometer
	Deployment boom		
	Other instruments		

As seen in Table 2.1, the subsystem components, especially the payload instruments, depend on the scope of the mission. Since the ST5 system comprises microsatellites, each satellite contains far more components in each subsystem than a CubeSat. However, there are some similarities between the components used in the three different systems. For example, all three contain the following:

- Battery
- Satellite bus/box
- Solar array

Additionally, the communications and GN&C subsystems were similar in function, even though the components themselves were different. The NASA Tropics and Hyperspectral systems especially have very similar components in their GN&C subsystem, such as an attitude determination system.

Nevertheless, the three constellation systems are not part of deep space missions. Since deep space CubeSats require more instruments and additional subsystems, their size would be at least 6U. Therefore, based on the information presented in Section 1.2.1, one example of a system decomposition of a deep space CubeSat can be as shown in Figure 2.1.

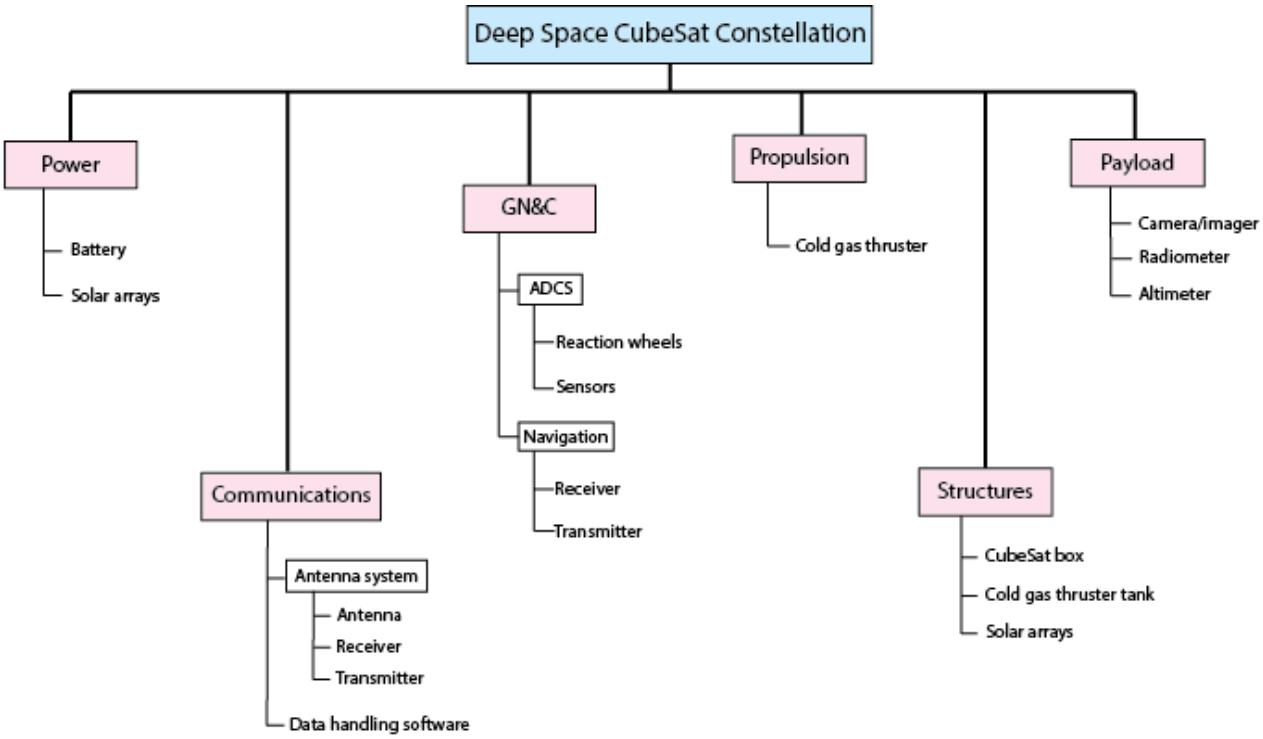

Figure 2.1 – System decomposition for deep space CubeSats.

The system decomposition in Figure 2.1 is similar to those of the constellation systems, save for their payload subsystems. Therefore, it shall be used as the system decomposition for this mission. The N2 diagram shown in Figure 2.2 shows the relationship between the subsystems.

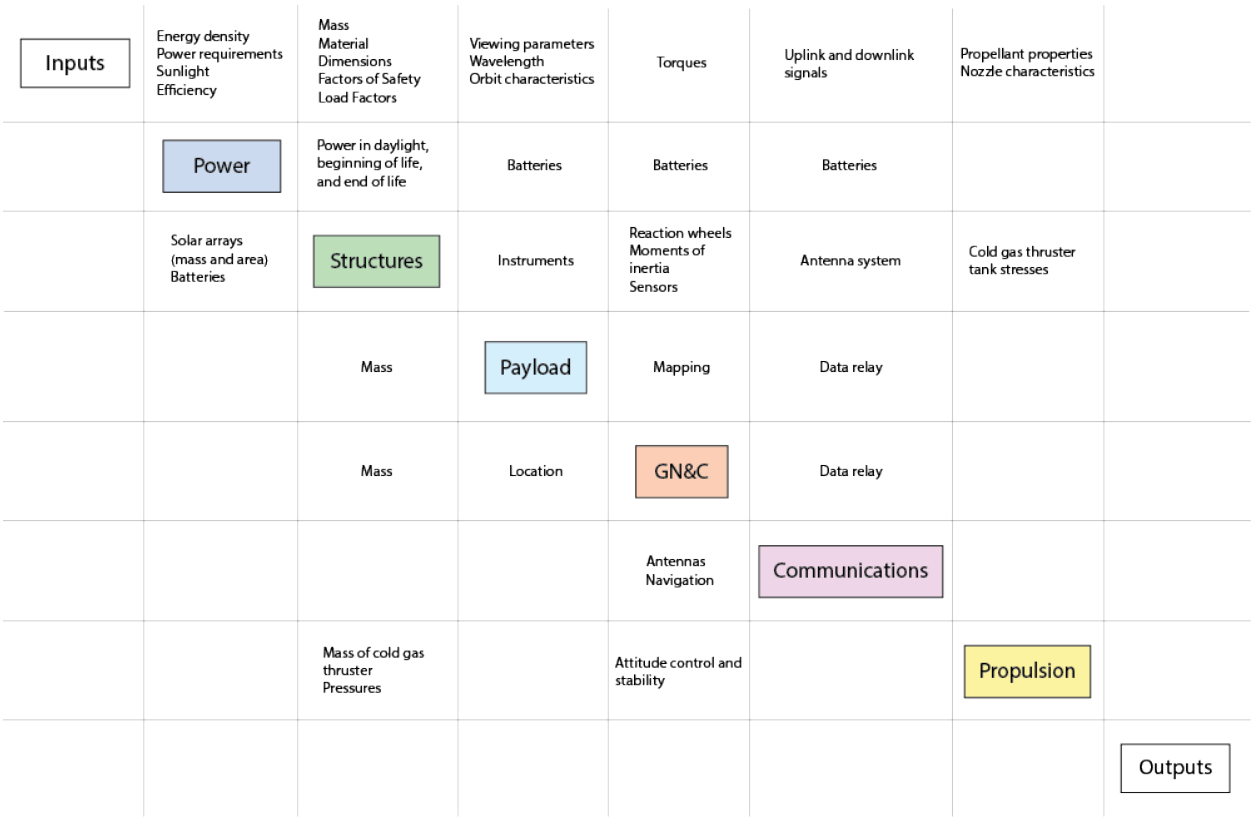

Figure 2.2 – N2 diagram of CubeSat constellation system.

Figure 2.2 above shows the subsystems arranged in a diagonal. The values above the diagonal represent the inputs to the subsystems below. The values below the diagonal represent the outputs of the subsystems on the right. For example, one input for the structures subsystem is the power in daylight, which is an output from the power subsystem. More information on each subsystem is found in the next section of this chapter.

2.2 SUBSYSTEMS AND COMPONENTS

This chapter will cover each subsystem and its components shown in both the system decomposition and N2 diagram above in more detail. Additionally, each of the following subsections will include relevant equations along with their inputs and outputs.

2.2.1 Power Subsystem

The power subsystem is primarily composed of the battery and solar arrays. The solar arrays provide power generation, and the battery provides power storage. Together, along with wires for power conversion and distribution, they form an EPS.

2.2.1.1 Power Generation from Solar Arrays

There are two main types of solar arrays: deployed and fixed. The power generation from the solar panels depends on the amount of sunlight received. Equation 2.1 is used to determine the amount of power needed from the solar array during daylight to power the spacecraft in orbit. Assume that battery charging losses are excluded.

$$P_{sa} = \frac{\left(\frac{P_e T_e}{X_e} + \frac{P_d T_d}{X_d}\right)}{T_d} \quad (2.1)$$

Inputs: P_e = Spacecraft's power requirement during eclipse,
P_d = Spacecraft's power requirement during daylight,
T_e = Period length of eclipse orbit,
T_d = Period length of daylight orbit,
X_e = Transmission efficiency during eclipse,
X_d = Transmission efficiency during daylight

Output: P_{sa} = Power needed from solar array during daylight

The efficiencies X_e and X_d depend on the type of power regulation, shown in Table 2.2 below.

Table 2.2: Transmission efficiencies for different types of power regulation.

	Type of Power Regulation	
Transmission Efficiencies	**Direct Energy Transfer**	**Peak-Power Tracking**
X_e	0.65	0.6
X_d	0.85	0.8

Efficiencies corresponding to direct energy transfer are larger because peak-power tracking requires a power converter between the solar arrays and the loads.

The beginning-of-life power per unit area P_{BOL} is calculated using Equation 2.2.

$$P_{BOL} = P_O I_d cos\,(\theta) \quad (2.2)$$

Inputs: P_O = Ideal solar cell performance,
I_d = Inherent degradation, 0.77 (nominal),
θ = Sun incidence angle, 23.5° for worst case, 90° for maximum power

Output: P_{BOL} = Beginning-of-life power per unit area

The ideal solar cell performance P_O depends on the type of solar cell used. By multiplying the solar flux with the efficiency value corresponding to the desired cell type in Table 2.3, the value for P_O can be found.

Table 2.3: Efficiencies for different types of solar cells.

Cell Type	**Efficiencies**
Silicon	0.148
Gallium Arsenide (GaAs)	0.185
Indium Phosphide	0.18
Multijunction GaInP/GaAs	0.22

The life degradation of the solar array L_d can be found using Equation 2.3.

$$L_d = (1 - degradation)^{satellite\ life} \quad (2.3)$$

Inputs: Degradation = solar cell degradation/year, 0.375 for silicon, 0.275 for GaAs,

Satellite life = usually length of the mission

Output: L_d = life degradation of the solar array

The end-of-life power per unit area P_{EOL} is calculated with Equation 2.4.

$$P_{EOL} = P_{BOL} L_d \tag{2.4}$$

Inputs: P_{BOL} = Beginning-of-life power per unit area,
L_d = life degradation of the solar array

Output: P_{EOL} = End-of-life power per unit area

2.2.1.2 Power Storage from Batteries

There are two types of battery cells: primary and secondary. Primary batteries are useful for short missions and tasks that use very little power. Secondary batteries are useful for long-term missions and can provide power during eclipse periods. Therefore, the CubeSats in this project's constellation system will use secondary batteries.

Secondary batteries are able to charge in sunlight and discharge during an eclipse. The required battery capacity C_r for each spacecraft can be estimated using Equation 2.5.

$$C_r = \frac{P_e \tau_e}{(DOD) N n} \tag{2.5}$$

Inputs: P_e = Spacecraft's power requirement during eclipse,
τ_e = Eclipse duration
DOD = depth of discharge, ranges from .20 to .80
N = number of batteries, between 2 and 5
n = transmission efficiency of the battery

Output: C_r = required battery capacity

The mass of the batteries can be calculated by dividing the battery capacity C_r by the specific energy density. Table 2.4 shows the specific energy densities for the different types of secondary battery couples.

Table 2.4: Specific energy densities for different types of secondary batteries [16].

Secondary Battery Type	**Specific Energy Density (W-hr/kg)**
Nickel-Cadmium (NiCd)	25 - 30
Nickel-Hydrogen, individual pressure vessel design (NiH)	35 - 43
Nickel-Hydrogen, common pressure vessel design (NiH)	40 - 56
Nickel-Hydrogen, common pressure vessel design (NiH)	43 - 57
Lithium-Ion (Li-Ion)	70 - 110
Sodium-Sulfur (NaS)	140 - 210

2.2.2 Communications Subsystem

The communications subsystem primarily includes an antenna system, as well as software to transmit data between the CubeSats in the constellation system and Earth. The antenna system contains an antenna, a transmitter, and a receiver. The transmitter sends downlink signals to the other satellites and the ground station. The receiver gets uplink signals from other satellites and the ground station.

The amount of data can be calculated using Equation 2.6.

$$DQ = \frac{DR \times (FT_{max} - T_{initiate})}{M} \quad (2.6)$$

Inputs: DR = data rate,
F = fractional reduction in viewing time,
T_{max} = maximum time in view,
$T_{initiate}$ = time required to initiate a communications pass,
M = margin needed to account for missed passes, estimated at 2 to 3

Output: DQ = quantity of data

The fractional reduction F will have a value greater than 0.5, and the initiation time $T_{initiate}$ can be estimated at 2 minutes. The data rate DR depends on the information relayed to and from the payload instruments. More information on the payload subsystem is found in Section 2.2.6.

Equation 2.7 can be used to size a data link.

$$\frac{E_b}{N_o} = 10\,log\left(\frac{PL_lG_tL_sL_aG_r}{kT_s(DR)}\right) \quad (2.7)$$

Inputs: P = transmitter power,
L_l = transmitter-to-antenna line loss,
G_t = transmit antenna gain,
L_s = space loss,
L_a = transmission path loss,
G_r = receive antenna gain,
k = Boltzmann's constant, 1.380 x 10^{-23} J/K,
T_s = system noise temperature,
DR = data rate

Output: E_b/N_o = ratio of received energy-per-bit to noise density

Usually, a ratio between 50 and 100 is acceptable. The expression PL_lG_t can also be expressed as the effective isotropic radiated power EIRP, which is related to the power flux density W_f. For an S-band antenna system, the W_f value is -137/4 kHz with the following uplink and downlink frequency ranges [16]:

- Uplink: 2.65 – 2.69 GHz
- Downlink: 2.5 – 2.54 GHz

Likewise, for an X-band antenna system, the W_f value is -142/4 kHz with the following uplink and downlink frequency ranges [16]:

- Uplink: 7.9 – 8.4 GHz
- Downlink: 7.25 – 7.75 GHz

For all of the uplink and downlink frequencies shown above for both types of antenna systems, the system noise temperatures T_s are as follows [16]:

- Uplink: 614 K
- Downlink: 135 K

Also, based on the frequencies, the transmission path loss L_a is -0.3 dB [16].

The space loss L_s can be found using Equation 2.8.

$$L_s = 20\,log\left(\frac{c}{4\pi Sf}\right) \tag{2.8}$$

Inputs: c = speed of light, 3 x 10^8 m/s
S = path length,
f = frequency

Output: L_s = space loss

The antenna pointing loss can be found using Equation 2.9.

$$L_\theta = -12\left(\frac{e}{\theta}\right)^2 \tag{2.9}$$

Inputs: e = pointing error,
θ = antenna half-power beamwidth

Output: L_θ = antenna pointing loss

The antenna half-power beamwidth θ used in Equation 2.9 can be calculated using

$$\theta = \frac{21}{f_{GHz}D} \tag{2.10}$$

Inputs: f = frequency in GHz,
D = antenna diameter

Output: θ = antenna half-power beamwidth

2.2.3 GN&C Subsystem

The GN&C subsystem mainly contains an ADCS system and a navigation system. The ADCS system contains sensors and actuators such as reaction wheels or torquers. The navigation system, similar to the communications subsystem, includes a receiver and transmitter. This section will focus more on the ADCS system design.

Based on other designs presented earlier, each spacecraft will use a spin stabilization control type, which uses passive control. The entire spacecraft rotates while the angular momentum vector remains fixed in space.

Reaction wheels in each ADCS system will act as the actuators to adjust orientation. They are able to spin in either direction, while providing one axis of control for each wheel. The following shows the typical specifications for reaction wheels [16].

- Weight: 2 – 20 kg
- Power: 10 – 110 W
- Performance Range: 0.01 to 1 N-m (max torque)

The sizing of the reaction wheels can be determined in two different ways. One way is to account for disturbance rejection in Equation 2.11.

$$T_{RW} = T_D(MF) \tag{2.11}$$

Inputs: T_D = worst-case disturbance torque,
MF = margin factor

Output: T_{RW} = reaction-wheel torque due to disturbance rejection

The disturbance torque T_D is caused by gravity gradients, solar radiation, magnetic fields, and aerodynamic disturbance. This relationship is shown in Equation 2.12 [16].[2]

$$T_D = T_G + T_{sp} + T_m + T_a \tag{2.12}$$

Inputs: T_G = maximum gravity torque,
T_{sp} = solar radiation torque,
T_m = magnetic torque,
T_a = aerodynamic torque

Output: T_D = worst-case disturbance torque

Another way to size the reaction wheels is to find the slew torque T_{slew} using Equation 2.13.

$$T_{slew} = \frac{4\theta I}{t^2} \tag{2.13}$$

Inputs: θ = slewing angle, 30 degrees,
I = moment of inertia of CubeSat,
t = minimum maneuver time

Output: T_{slew} = slew torque

The wheel momentum h can be estimated using Equation 2.14.

$$h = \frac{T_D \tau}{4\sqrt{2}} \tag{2.14}$$

Inputs: T_D = disturbance torque,
τ = orbit period

Output: h = wheel momentum

Both Sun sensors and gyroscopes (inertial sensors) will also be used to supplement the CubeSats' navigation system. Sun sensors use visible light to measure angles between their mounting base and incident sunlight. Gyroscopes can be used with Sun sensors to measure the speed or angle of rotation from an initial reference. The following shows characteristics for both Sun sensors and gyroscopes [16].

- Weight Range: 1 to 15 kg (gyro), 0.1 to 2 kg (Sun sensor)
- Power: 10 to 200 W (gyro), 0 to 3 (Sun sensor)
- Performance: Gyro drift rate 0.003 to 1 deg/hr, sun sensor accuracy 0.005 to 3 deg

[2] [16], Table 11-9A

2.2.4 Propulsion Subsystem

The main component in the propulsion subsystem is the cold gas thruster due to its low cost and simplicity. The propellant (N2, NH3, Freon, He) performance characteristics are as follows [16]:

- Vacuum specific impulse (I_{sp}): 50-75 seconds
- Thrust range (F): 0.05-200 N
- Average bulk density: 0.28, 0.60, and 0.96 g/cm^3

Other types of propulsion systems are not needed for constellation systems because the subsystem would only be required to maintain attitude control and orbit maintenance and maneuvering. Therefore, staging will not be considered for this project. Since a single thruster has such a low specific impulse, multiple will need to be used.

Figure 2.3 shows a schematic of a single cold gas thruster propulsion system.

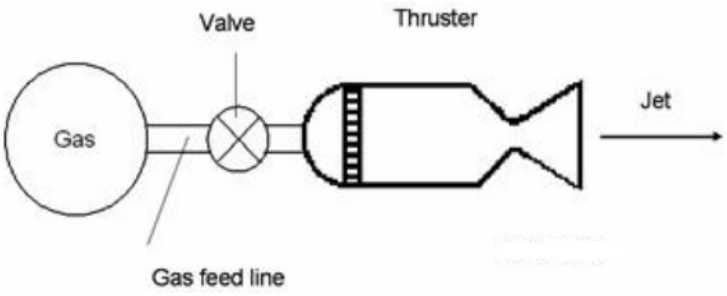

Figure 2.3 – Schematic of cold gas propulsion system [17].

As seen in Figure 2.2, the propulsion system consists of a gas tank, gas feed line, valve, and thruster. The gas tank is either cylindrical or spherical in shape. Relevant equations, inputs, and outputs relating to its structure will be presented in a later section.

The thruster itself is a convergent-divergent nozzle. Key assumptions for the nozzle design include the following:

- The flow is isentropic, quasi, and one-dimensional
- The propellant is an ideally, thermally, calorically perfect gas

Equation 2.15 is used to find the thrust generated by the system.

$$F = \dot{m}V_e + A_eP_e \tag{2.15}$$

Inputs: ṁ = propellant mass flow rate,
V_e = propellant exhaust velocity,
A_e = nozzle exit area,
P_e = gas pressure at nozzle exit

Output: F = thrust

The thrust is used to find the specific impulse, shown in Equation 2.16.

$$I_{sp} = \frac{F}{\dot{m}g} \tag{2.16}$$

Inputs: F = thrust,
ṁ = propellant mass flow rate,

g = acceleration due to gravity, 9.81 m/s^2

Output: I_{sp} = specific impulse

The propellant exhaust velocity V_e can be found using Equation 2.17.

$$V_e = \sqrt{\frac{2\gamma}{\gamma-1}\left(\frac{R_A}{M_W}\right)T_c\left(1-\left(\frac{P_e}{P_c}\right)^{\frac{\gamma-1}{\gamma}}\right)} \qquad (2.17)$$

Inputs: γ = specific heat ratio for gas,
R_A = universal gas constant, 8.314 J/K-mol,
M_W = molecular weight of gas,
T_c = chamber temperature,
P_e = gas pressure at nozzle exit
P_c = chamber pressure

Output: V_e = propellant exhaust velocity

The nozzle's area expansion ratio ε can be found using Equation 2.18.

$$\varepsilon = \frac{A_e}{A_t} \qquad (2.18)$$

Inputs: A_e = nozzle exit area,
A_t = nozzle throat area

Output: ε = area expansion ratio

The characteristic velocity c* can be found using Equation 2.19.

$$c^* = \frac{P_c A_t}{\dot{m}} \qquad (2.19)$$

Inputs: P_C = chamber pressure,
A_t = nozzle throat area,
$\dot{m}$ = propellant mass flow rate

Output: c* = characteristic velocity

The thrust coefficient c_f can be found using Equation 2.20.

$$c_f = \frac{F}{P_c A_t} \qquad (2.20)$$

Inputs: F = thrust,
P_c = chamber pressure,
A_t = nozzle throat area

Output: c_f = thrust coefficient

Both the characteristic velocity c* and the thrust coefficient c_f are used to evaluate the performance of the propulsion system.

2.2.5 Structures Subsystem

The primary component of the structures subsystem is the CubeSat box. Other components include the cold gas thruster tank and other components of the other subsystems. Basic analysis will mainly be done on the CubeSat box, cold gas thruster tank, and solar arrays.

2.2.5.1 CubeSat Box

The CubeSat box will have a monocoque structure and will be made of aluminum 7075-T73 sheets. This type of material is most often used for spacecraft due to its easy machinability, ductility, low density, and high strength versus weight. The following material properties will be useful in conducting structural analysis for the main CubeSat box [16].

- Young's Modulus: $E = 71 \times 10^9$ N/m^2
- Poisson's Ratio: $\nu = 0.33$
- Density: $\rho = 2.8 \times 10^3$ kg/m^3
- Ultimate Tensile Strength: $F_{tu} = 524 \times 10^8$ N/m^2
- Yield Tensile Strength: $F_{ty} = 448 \times 10^6$ N/m^2

Assuming uniform thickness, Equations 2.21 and 2.22 can be used to find the axial frequency $f_{nat,a}$ and lateral frequency $f_{nat,l}$.

$$f_{nat,a} = 0.250\sqrt{\frac{AE}{m_B L}} \tag{2.21}$$

$$f_{nat,l} = 0.560\sqrt{\frac{EI}{m_B L^3}} \tag{2.22}$$

Inputs: A = cross-sectional area of CubeSat box,
E = Young's Modulus,
m_B = estimated distributed mass of CubeSat box,
L = length of CubeSat box,
I = area moment of inertia

Outputs: $f_{nat,a}$ = axial frequency,
$f_{nat,l}$ = lateral frequency

The estimated distributed mass of the CubeSat box m_B includes the box itself, as well as the components located inside.

The area moment of inertia for the CubeSat box can be found using Equation 2.23.

$$I = \frac{bh^3}{12} \tag{2.23}$$

Inputs: b = base of cross section,
h = height of cross section

Output: I = area moment of inertia

The limit load, or the equivalent axial load P_{eq}, can be found using Equation 2.24.

$$P_{eq} = m_B g(LF) + \frac{4M}{b} \tag{2.24}$$

Inputs: m_B = estimated distributed mass of CubeSat box,

g = acceleration due to gravity, 9.81 m/s^2,
LF = loading factor,
M = bending moment,
b = base of cross section

Output: P_{eq} = equivalent axial load

The bending moment used in Equation 2.24 can be calculated using Equation 2.25.

$$M = m_B g y \tag{2.25}$$

Inputs: m_B = estimated distributed mass of CubeSat box,
g = acceleration due to gravity, 9.81 m/s^2,
y = moment arm, or distance from center of mass

Output: M = bending moment

The ultimate and yield equivalent axial loads ($P_{eq,u}$ and $P_{eq,y}$, respectively) can be found using their respective factors of safety FS_u and FS_y, shown in Equation 2.26.

$$P_{eq,u} \; or \; P_{eq,y} = P_{eq} \times (FS_u \; or \; FS_y) \tag{2.26}$$

Inputs: P_{eq} = equivalent axial load,
FS_u or FS_y = ultimate or yield factor of safety

Output: $P_{eq,u}$ or $P_{eq,y}$ = ultimate or yield equivalent axial load

The factors of safety depend on the type of structure being designed. Since the CubeSat box is being designed for strength and will be affected by temperature changes during the mission, the factors of safety will be as follows [16]:

- Ultimate factor of safety $FS_u = 1.25$
- Yield factor of safety $FS_y = 1.1$

The critical buckling load P_{cr} for the structure is calculated using Equation 2.27.

$$P_{cr} = \frac{\pi^2 EI}{4L^2} \tag{2.27}$$

Inputs: E = Young's Modulus,
I = area moment of inertia,
L = length of CubeSat box

Output: P_{cr} = critical buckling load

Both the ultimate equivalent axial load P_{eq} and critical buckling load P_{cr} are used in Equation 2.28 to determine the stability of the structure.

$$MS = \frac{P_{cr}}{P_{eq}} - 1 \tag{2.28}$$

Inputs: P_{cr} = critical buckling load,
P_{eq} = equivalent axial load

Output: MS = margin of safety

If the margin of safety MS is less than zero, then the structure is not adequate for the mission. The inputs to calculate the applied loads will need to be modified until the margin of safety MS is greater than or equal to zero.

The mass of the box's shell m_{box}, not including fasteners or attachments, is calculated using Equation 2.29.

$$m_{box} = \rho \forall \quad (2.29)$$

Inputs: ρ = density of material,
$\forall$ = volume of CubeSat box only

Output: m_{box} = mass of CubeSat box shell only

2.2.5.2 Gas Tank

The structural design of the tank depends on its shape. As described in Section 2.2.3, a tank for a cold gas thruster system is either cylindrical or spherical in shape. Equation 2.30 is used to find the spherical tank stress.

$$\sigma = \frac{Pr}{2t} \quad (2.30)$$

Inputs: P = maximum expected operating pressure,
r = radius,
t = thickness

Output: σ = allowable stress

Cylindrical pressure vessels depend on both the longitudinal and hoop stresses. Equation 2.30 can be used to find the longitudinal stress of a cylindrical pressure vessel, and Equation 2.31 can be used to find the hoop stress.

$$\sigma = \frac{Pr}{t} \quad (2.31)$$

Inputs: P = maximum expected operating pressure,
r = radius,
t = thickness

Output: σ = allowable stress

2.2.5.3 Solar Arrays

Using the values calculated in Section 2.2.1.1, the size of the solar arrays can be found. Equation 2.32 is used to calculate the solar-array area A_{sa} needed to support each spacecraft's power requirement.

$$A_{sa} = \frac{P_{sa}}{P_{EOL}} \quad (2.32)$$

Inputs: P_{sa} = Power needed from solar array during daylight,
P_{EOL} = End-of-life power per unit area

Output: A_{sa} = required solar-array area

The mass of the solar arrays can also be found using Equation 2.33.

$$m_a = 0.04P_{sa} \tag{2.33}$$

Input: P_{sa} = Power needed from solar array during daylight

Output: m_a = mass of solar arrays

2.2.6 Payload Subsystem

The payload subsystem is made up of different instruments and depends on the type of mission and mission objective. Therefore, it drives the mission requirements and specifications. For a deep space, remote sensing mission such as this project, the instruments would be required to perform imaging, intensity measurement, and topographic mapping. Therefore, the payload would include an imager/camera, radiometer, and altimeter used for analysis in deep space [16].

The data rate DR used as an input for the communications subsystem can be calculated using Equation 2.34.

$$DR = Z_C Z_A B \tag{2.34}$$

Inputs: Z_C = Number of cross-track pixels,
Z_A = Number of swaths in one second
B = Number of bits per pixel

Output: DR = data rate

The number of cross-track pixels Z_C can be calculated using Equation 2.35.

$$Z_C = \frac{2\eta}{IFOV} \tag{2.35}$$

Inputs: η = maximum sensor look angle,
IFOV = Instantaneous field of view

Output: Z_C = Number of cross-track pixels

The number of swaths Z_A can be calculated using Equation 2.36.

$$Z_A = \frac{V_g \times 1\ sec}{IFOV \times H\left(\frac{\pi}{180^\circ}\right)} \tag{2.36}$$

Inputs: V_g = spacecraft ground-track velocity,
IFOV = Instantaneous field of view,
H = orbit altitude

Output: Z_A = Number of swaths in one second

The instantaneous field of view IFOV can be calculated using Equation 2.37.

$$IFOV = \frac{Y_{max}}{R_s}\left(\frac{180^\circ}{\pi}\right) \tag{2.37}$$

Inputs: Y_{max} = maximum along-track ground sampling distance,
R_s = slant range

Output: IFOV = Instantaneous field of view

The pixel integration period τ_i, a parameter for sensor integration, can be found using Equation 2.38.

$$\tau_i = \frac{N_m IFOV \times H\left(\frac{\pi}{180^\circ}\right)}{V_g Z_c} \quad (2.38)$$

Inputs: N_m = Number of pixels on instrument scanner,
$IFOV$ = Instantaneous field of view,
H = orbit altitude,
V_g = spacecraft ground-track velocity,
Z_C = Number of cross-track pixels

Output: τ_i = pixel integration period

The aperture diameter D, a parameter for sensor optics and imaging, can be found using Equation 2.39

$$D = \frac{2.44 \lambda f Q}{d} \quad (2.39)$$

Inputs: λ = operating wavelength,
f = focal length,
Q = quality factor for imaging,
d = width for square detectors

Output: D = aperture diameter

The aperture diameter of both the instrument used in the system and a similar instrument can be used as a ratio R to then estimate the size, weight, and power. Those can be calculated using Equations 2.40, 2.41, and 2.42.

$$V_i = (R L_o)^3 \quad (2.40)$$

$$W_i = K R^3 W_o \quad (2.41)$$

$$P_i = K R^3 P_o \quad (2.42)$$

Inputs: R = aperture ratio (new instrument to similar instrument),
L_o = linear dimensions of similar instrument,
K = factor, equal to 2 if $R < 0.5$, equal to 1 otherwise,
W_o = weight of similar instrument,
P_o = power of similar instrument

Outputs: V_i = volume of new instrument,
W_i = weight of new instrument,
P_i = power of new instrument

3. ORBITAL MECHANICS AND CONSTELLATION DESIGN

In designing a constellation system, several key design factors need to be considered:

- Number of satellites
- Constellation pattern
- Altitude
- Number of orbit planes
- Minimum elevation angle
- Inclination
- Eccentricity
- Collision avoidance parameters (i.e. spacing between satellites)

Of those listed above, the three most important are the altitude, inclination, and minimum elevation angle. The altitude and minimum elevation angle can be assumed as design variables, while the inclination depends on either analytical calculations or constellation pattern.

This section will cover both general orbital mechanics and the constellation system structure. In designing the constellation structure, all assumptions listed in Section 1.2.2.4 will be considered. Therefore, the following will be true for this project:

1. Since the planet or moon will be considered a round body, no oblate body perturbations will be incorporated. However, other perturbations such as solar radiation or finite burns may be incorporated depending on their relevance to the mission.
2. All satellites will be at the same altitude, and each orbit plane will contain the same number of satellites.
3. All orbit planes will have the same inclination, either determined through analytical calculations or the chosen constellation pattern.

3.1 FORCES AND PERTURBATIONS

To better simulate reality, different outside forces or perturbations must be considered. For example, solar pressure and atmospheric drag can affect the values of the orbits' Keplerian elements, which will be discussed in Section 3.2. Finite burns, however, have low impact on orbital changes but should still be considered [16,18].

The final design will incorporate more than two bodies in the reference frame, including the other CubeSats in the constellation system. For now, this will be a two-body problem that will consider only the primary CubeSat and the planet or moon. Equation 3.1 shows the general equation of motion for the two-body problem.

$$m\frac{d^2}{dt^2}\boldsymbol{r^Q} = -\frac{GMm}{r^3}\boldsymbol{r^Q} + \boldsymbol{p_Q} \qquad (3.1)$$

Both inputs and outputs are forces. The perturbation force vector $\mathbf{p_Q}$ accounts for all external forces considered in the two-body problem.

3.1.1 Finite Burns

Finite burns are usually assumed as instantaneous, since the burn to adjust a CubeSat's course is very brief. The scalar quantity of the perturbation force can be modeled as the thrust, which can be found using Equation 2.15. Then, the thrust vector can be found using Equation 3.2.

$$\boldsymbol{p_{thrust}} = F\frac{\boldsymbol{v^Q}}{|\boldsymbol{v^Q}|} \quad (3.2)$$

Inputs: F = thrust,
$\mathbf{v^Q}$ = velocity vector of the satellite

Output: $\mathbf{p_{thrust}}$ = thrust perturbation vector of the satellite

3.1.2 Atmospheric Drag

Drag perturbations are only considered for low altitudes (below 800 km) over planets or moons with an atmosphere, so they should only be considered if necessary. The drag scalar can be found using Equation 3.3.

$$p_{drag} = -\frac{1}{2}\rho v_{satellite}^2 C_D A \quad (3.3)$$

Inputs: ρ = density of atmosphere,
$v_{satellite}$ = velocity of the satellite,
C_D = coefficient of drag,
A = cross-sectional area of satellite

Output: p_{drag} = drag scalar of the satellite

The vector quantity acts in the opposite direction of the velocity vector, or opposite to the thrust vector.

3.1.3 Solar Radiation

When compared to atmospheric drag, perturbations due to solar radiation are much smaller at low altitudes. However, at higher altitudes (above 800 km), they should be considered more than drag perturbations. The solar radiation perturbation can be found using Equation 3.4.

$$p_{radiation} = (-4.5 \times 10^{-6})(1 - r)A \quad (3.4)$$

Inputs: r = reflection factor (0 for absorption, 1 for specular reflection, 0.4 for diffuse reflection),
A = cross-sectional area of satellite

Output: $p_{radiation}$ = solar radiation perturbation

3.2 KEPLERIAN ELEMENTS

The satellites' orbits are generally defined by the Keplerian elements, which are as follows [18]:

- Length of semi-major axis, a
- Eccentricity, e
- Argument of periapsis, ω
- True anomaly, θ
- Inclination, i
- Right ascension of ascending node, Ω

The latter four elements are illustrated in Figure 3.1. Note that the equatorial plane shown in the illustration below is of the Earth.

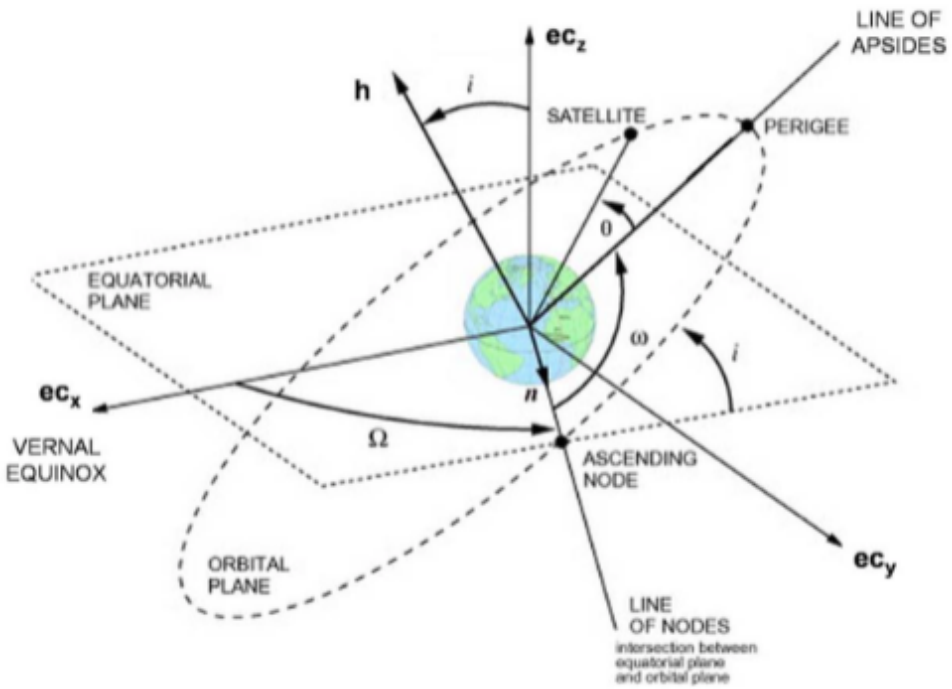

Figure 3.1 – Orientation of orbit plane with respect to equatorial plane.

For both types of coverage, continuous or discontinuous, the orbits can be assumed as circular, due to its more widespread use than elliptical ones [2]. Therefore, the semi-major axis is equal to the radius of the orbit, which is the sum of the altitude and the radius of the planet or moon. For circular orbits, the eccentricity is equal to zero.

Additionally, the true anomaly and the argument of periapsis can be combined to obtain the argument of latitude u. This is because both angles depend on the Line of Apsides, which does not exist for circular orbits [16,19]. The argument of latitude can be any value ranging from 0 to 360 degrees [19].

In place of the true anomaly, the orbital period can be considered as another Keplerian element. Using the semi-major axis, the orbital period τ can be found using Equation 3.1 [18].

$$\tau = 2\pi\sqrt{\frac{a^3}{GM}} \tag{3.5}$$

Inputs: a = length of semi-major axis,
G = gravitational constant, 6.67 x 10^{-20} $km^3/kg\text{-}s^2$,
M = mass of the planet or moon

Output: τ = orbital period

The remaining two Keplerian elements depend on the type of constellation structure, discussed in Section 3.2. The inclination, in particular, depends on the angular momentum, which is found using Equation 3.3.

$$h = a \times v_{satellite} \tag{3.6}$$

Inputs: a = length of semi-major axis,

$v_{satellite}$ = velocity of the satellite

Output: h = angular momentum of the satellite

If an inclination angle is not otherwise determined due to the selection of the constellation structure, it can be found using Equation 3.4.

$$i = cos^{-1}\left(\frac{h_z}{h}\right) \quad (3.7)$$

Inputs: h_z = z-component of angular momentum vector,[3]
h = angular momentum of the satellite

Output: i = inclination angle

The right ascension of the ascending node depends on the Line of Nodes, which also depends on the angular momentum. Equation 3.5 can be used to find the right ascension of the ascending node.

$$\Omega = cos^{-1}\left(\frac{-h_y}{n}\right) \quad (3.8)$$

Inputs: h_y = y-component of angular momentum vector,[4]
n = magnitude of the Line of Nodes[5]

Output: Ω = right ascension of the ascending node

3.3 CONSTELLATION STRUCTURE

The structure of a constellation system is symmetric; therefore, there should be an equal number of satellites in each orbit plane. Usually, constellations with one or two planes are more responsive to changes based on user needs than those with more than two [16]. Therefore, it is better to place more satellites in a smaller number of planes rather than placing less satellites in a larger number of planes. Nevertheless, the structure and number of constellation planes should allow for maximum coverage with the smallest possible number of satellites.

There are two common types of constellation structures that use circular orbit patterns:

- Streets of Coverage pattern
- Walker-Delta pattern

Figure 3.2 shows an example of a Streets of Coverage pattern.

[3] Calculation for the angular momentum vector is shown in Appendix A.
[4] Calculation for the angular momentum vector is shown in Appendix A.
[5] Line of Nodes calculation is shown in Appendix A.

Figure 3.2 – Streets of Coverage pattern, i = 90° [16].

Planes in the Streets of Coverage pattern all have the same inclination at 90 degrees, since it is a polar constellation [20]. One main advantage is that most of the orbital planes in this pattern are evenly spaced, so they have similar Ω values. The example shown in Figure 3.2 uses five planes in the pattern, all intersecting at the poles. The image shows the main disadvantage of this pattern; coverage is more concentrated in areas closer to the poles than the equator [16,20].

Figure 3.3 shows an example of a Walker-Delta pattern.

Figure 3.3 – Walker-Delta pattern at i = 65° [16].

Planes in the Walker-Delta pattern all have the same inclination relative to the equatorial plane, which allows for equally distributed coverage everywhere over the surface. The example shown in Figure 3.3 uses 15 satellites in total, distributed across five planes. Each plane is at an inclination of 65 degrees with respect to the equator.

However, one main disadvantage of the Walker-Delta pattern is its design constraints; both the orbital planes and satellites have to be equally spaced from each other, which adds more difficulty in optimizing the design [20]. Therefore, for maximum coverage and simplicity, the constellation

system for this project will use the Streets of Coverage pattern. Figure 3.4 shows a view of the example shown in Figure 3.2 from the north pole.

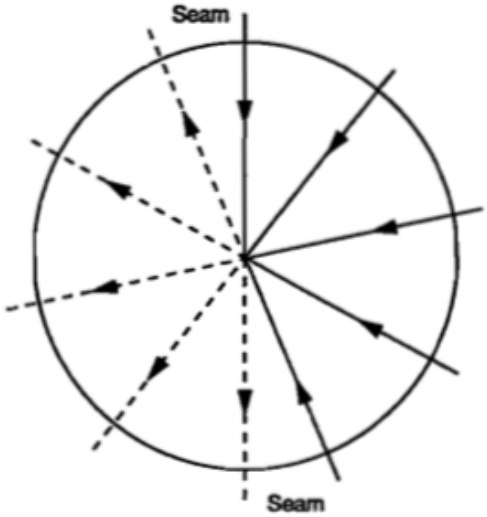

Figure 3.4 – Streets of Coverage pattern view from north pole [16].

Satellites traveling over half of the planet or moon travel northward, while those over the other half travel southward. Equation 3.6 is used to calculate the maximum perpendicular separation between two adjacent orbital planes going in the same direction.

$$D_{max_S} = \lambda_{street} + \lambda_{max} \tag{3.9}$$

Inputs: λ_{street} = street of coverage angle,
λ_{max} = maximum central angle

Output: D_{maxS} = maximum perpendicular separation between two adjacent orbital planes going in the same direction

There is a seam between the two halves in Figure 3.4, which has much narrower spacing than other areas in the pattern. The Ω values for those two planes will be different from those of the other planes. Equation 3.7 is used to calculate the maximum perpendicular separation between two adjacent orbital planes going in opposite directions.

$$D_{max_O} = 2\lambda_{street} \tag{3.10}$$

Input: λ_{street} = street of coverage angle

Output: D_{maxO} = maximum perpendicular separation between two adjacent orbital planes going in opposite directions

The "street of coverage" is an area or swath with continuous coverage that is centered on the ground track. The street of coverage angle, half of the width of a swath, depends on both the space between satellites in each plane and the maximum central angle. This relationship is shown in Equation 3.8.

$$cos(\lambda_{street}) = \frac{cos(\lambda_{max})}{cos\left(\frac{S}{2}\right)} \tag{3.11}$$

Inputs: λ_{max} = maximum central angle,
S = space between satellites in each plane[6]

Output: λ_{street} = street of coverage angle

The relationships between both the maximum central angle and space between satellites help determine whether coverage is continuous or discontinuous, which are as follows:

- If $S < 2\lambda_{max}$, then coverage in the swath is continuous.
- If $S > 2\lambda_{max}$, then coverage in the swath is discontinuous.

Using the number of satellites per plane N_P, Equation 3.8 can be used to find the revisit time t_{rev} for discontinuous coverage [4].

$$t_{rev} = \frac{\tau}{N_P} \tag{3.12}$$

Inputs: τ = orbital period,
N_P = number of satellites per plane

Output: t_{rev} = revisit time

The revisit time is useful for adding extra coverage over certain areas such as the equator, the poles, and various terrains.

[6] This is found by dividing 360 degrees by N_P.

4. DESIGN OPTIMIZATION AND ANALYSIS

The equations presented in Chapters 2 and 3 will be used to determine key design parameters for the individual CubeSats and constellation system. These design parameters will help determine the best design scenarios for the system. Additionally, the design parameters of the overall constellation system will be used to generate simulations presented in Chapter 5. Microsoft Excel was used for calculations in this project. Results from sample calculations, which use Mars as the central body, will also be discussed in each section.

Outside forces and perturbations were not calculated for this section. Instead, they will be directly added through the simulation software.

4.1 ANALYSIS OF INDIVIDUAL CUBESATS

This section will discuss design parameters and analysis for each subsystem. Additional formulas used for calculations are shown in the Appendix.

4.1.1 Power Subsystem Analysis

The power subsystem depends mainly on the spacecraft life, solar array characteristics, and orbit characteristics. Each CubeSat can be assumed to have a lifespan of two to four years, since they should function in deep space. If the lifespan is higher, then both L_d and P_{BOL} are lower. Both P_e and P_d can be assumed to be a fixed power of 14 W, taken from literature review.

For all solar array calculations, peak-power tracking was used for power regulation. Therefore, P_{sa} is higher than if direct energy transfer was used. Both P_{BOL} and P_{EOL} depend on the type of solar cell used. GaAs solar cells have the best efficiency and the lowest degradation, and they contribute to the best P_{BOL} and P_{EOL} results.

The batteries used for the CubeSats in this project are based on those used on MarCO. Li-Ion batteries are predominantly used on CubeSats today because they are rechargeable, light, and have a high specific energy density. Each CubeSat will contain two Li-Ion batteries, with a total battery mass of around 0.7 kg.

The orbit characteristics, which include the eclipse duration and solar flux, depend on the central body. If the central body has a smaller angular radius, then the eclipse duration is smaller. Additionally, if the central body is farther from the Sun, then the solar flux is smaller. These characteristics are determined concurrently with simulation results.

Table 4.1 shows results from the sample calculations along with explanations for each.

Table 4.1: Power subsystem sample results.

Results	Values	Comments
P_{sa}	41.027 W	Orbit around Mars, peak-power tracking
P_{BOL}	77.075 W	Mars solar flux, GaAs solar cell type
L_d	0.381 year	CubeSat life of 3 years
P_{EOL}	29.372 W	
C_r	191.49 W-hr	Battery capacity for each battery
Mass of batteries	0.723 kg/battery	Li-Ion battery type

4.1.2 Communications Subsystem Analysis

The communications subsystem indirectly depends on orbit characteristics, since one of the design parameters is the payload's data rate. The size and performance in the communications instruments will be based on similar ones in other CubeSat missions.

An X-band antenna system has higher frequency ranges for both uplink and downlink, but those frequencies can contribute to a higher L_θ if there is a pointing error. However, this type of antenna system was used on MarCO, so it will be used in this mission.

Table 4.2 shows the results using the desired antenna system and other parameters.

Table 4.2: Communications subsystem sample results.

Results	Values	Comments
DQ	27871800 bits	DR = 31529 bps (see Section 4.1.6), F = 0.77, maximum time is 1 hour
E_b/N_o (uplink)	225 dB	Frequency = 7.9 GHz
E_b/N_o (downlink)	231 dB	Frequency = 7.25 GHz
L_θ (uplink)	-16982 dB	D = 1 mm, pointing error of 0.0001
L_θ (downlink)	-14303 dB	

The E_b/N_o ratio for both uplink and downlink is more than two times higher than the desired value, probably due to the data rate. Still, it is higher for the downlink than the uplink. The downlink L_θ is less than that of the uplink.

4.1.3 GN&C Subsystem Analysis

The orbit characteristics, especially those of the central body, greatly impact the sizing of the reaction wheels of the GN&C subsystem. As mentioned earlier, their sizing is determined by T_{RW} or T_{slew}. The wheel momentum is found through T_D and T_{slew}.

If the central body has little to no impact on the CubeSat's magnetic or aerodynamic torque, then T_{slew} should be used as a design parameter. Otherwise, T_{RW} must be compared with the maximum torque (0.01 to 1 N-m) to determine the better design parameter. If T_{RW} is less than the maximum torque, then T_{slew} must be considered as the main design parameter for the reaction wheel torque.

Table 4.3 shows T_{RW}, T_{slew}, and the wheel momentum for a CubeSat orbiting Mars.

Table 4.3: GN&C subsystem sample results.

Results	Values	Comments
T_{RW}	1.098×10^{-6} N-m	Mainly influenced by solar radiation and aerodynamic torques
T_{slew}	1.396×10^{-6} N-m	Min maneuver time of 5 seconds
Wheel momentum	0.001433 N-m-s	

As seen in the table above, T_{RW} is less than the maximum torque and T_{slew}. Therefore, T_{slew} should be the main design parameter for the reaction wheel torque. Additionally, the wheel momentum is very small; therefore, the mass of the reaction wheels should be less than 2 kg.

4.1.4 Propulsion Subsystem Analysis

The performance of the propulsion system depends on the propellant used. Therefore, the major design variables are the thrust, specific impulse, molecular weight, and specific heat ratio. Out of the four propellants mentioned, N2 and NH3 produce the best results because of their light weight and lower specific heat ratio. NH3 has the best of the two, since it produces the highest exhaust velocity. Therefore, the propulsion system in each CubeSat will use NH3 as its propellant, which has the following characteristics:

- $\gamma = 1.32$
- MW = 0.01703 kg/mol

The size and other characteristics of the cold gas thruster is based on similar models used on other CubeSats. For this project, the area ratio of the nozzle will be 50. Since a cold gas thruster has lower performance than other propulsion systems, the chamber temperature will be relatively low (between 200 and 320 K). The higher the chamber temperature, the higher the exhaust velocity.

Table 4.4 shows results using the selected propellant.

Table 4.4: Propulsion subsystem sample results.

Results	Values	Comments
V_e	790.5 m/s	Assume chamber and exit conditions to be T_c = 300 K, P_c = 800 kPa, P_e = 40 kPa
$\dot{m}$	-2.53 kg/s	F = 0.05 N, I_{sp} = 50 seconds
c*	-316.213 m/s	Assume $A_t = 0.001$ m^2, $A_e = 0.05$ m^2
c_F	0.167	

4.1.5 Structures Subsystem Analysis

Parameters for CubeSat structure depend on the m_B of the box, which includes the mass of the propulsion system, batteries, and other instruments. The mass of the solar arrays are not included, since they are not stored inside the box. The mass of the box shell is around 16.8 kg, so the distributed mass should be assumed greater than that. For calculations, m_B is assumed to be around 25 kg as the maximum possible mass.

Given a maximum operating pressure and gas tank thickness, a spherical tank would have a lower allowable stress than a cylindrical tank's hoop stress. However, a spherical tank is more structurally stable than a cylindrical one, since there are no edges. Therefore, the gas tank for the cold gas thruster system will be spherical. Using an average bulk density of .96 g/cm^3 and volume of the tank, the propellant mass is found to be around .025 kg.

Both the area and the mass of the solar arrays strongly depend on the design parameters of the power subsystem. The area depends on the type of solar cells used; GaAs solar cells contribute to a smaller area, which still makes them the best choice for the solar arrays. The mass, on the other hand, depends on the power required and orbit characteristics. Using the given power requirement, the area and mass are less than 2 m^2 and 2 kg, respectively.

4.1.6 Payload Subsystem Analysis

Payload instruments are based on similar ones in other CubeSat missions due to the size, weight, and power requirements. Therefore, the most important calculation for this subsystem was the data rate, which depends on the orbit altitude and spacecraft speed. This also influences the maximum

sensor look angle, which is an important parameter in the constellation system. A higher spacecraft speed gives a higher number of swaths in one second, which then leads to a higher date rate. From the sample calculations, the data rate was found to be around 32327 bps.

4.2 ANALYSIS OF CONSTELLATION SYSTEM

The velocity and orbital period of each spacecraft affect subsystems such as communications, GN&C, and the payload. The scalar angular momentum can be found using the velocity. The following orbit parameters were determined in Chapter 3:

- Eccentricity, e = 0
- Inclination, i = 90 degrees

With the inclination shown above, the z component of the angular momentum vector is found to be zero. Therefore, the scalar angular momentum is equal to the magnitude of the Line of Nodes. Other orbit parameters, u and Ω, are determined based on the size of the swaths and the space between the satellites.

Using Mars as the central body and an orbit altitude of 500 km, the following parameters are found:

- τ = 7386 seconds
- $v_{satellite}$ = 3.314 km/s
- h = 12914 km^2/s

The constellation system will have between three and five planes for maximum possible coverage and simplicity. Constellation design parameters such as the number of satellites and space between satellites depend on the desired amount of coverage and the radius of the central body. Each plane should have a minimum of nine satellites per plane, so that coverage within a swath can be continuous. A higher number of satellites per plane leads to lower revisit time.

The sample calculations assume 3 planes with 18 satellites in each. Table 4.5 shows the resulting parameters for the simulation.

Table 4.5: Sample constellation parameters, N_P = 18, 3 planes.

Parameters	**Values**	**Comments**
S	20 degrees	For satellites within each plane
t_{rev}	410.3 seconds	For discontinuous coverage
λ_{max}	20.9 degrees	Assume 10° elevation angle, Coverage in swath is continuous
λ_{street}	18.4 degrees	
$D_{max,S}$	39.26 degrees	Size of swaths away from seam
$D_{max,O}$	36.8 degrees	Size of swaths near seam

The parameters above will be used to generate a simulation. Other simulations will also be done to show constellations with different number of satellites per plane.

5. SIMULATIONS

This section presents three different simulations, each with different Ω and u values for each orbit. The first simulation uses data presented in Section 4.2, while the other two are shown with their respective constellation data. All other inputs (i.e. CubeSat communications parameters) are the same for all three simulations.

Simulations were developed using AGI's Systems Tool Kit (STK).

5.1 SAMPLE CONSTELLATION SYSTEM

Using the parameters shown in Table 4.5, Figure 5.1 shows a top view of the constellation system at the start of the simulation.

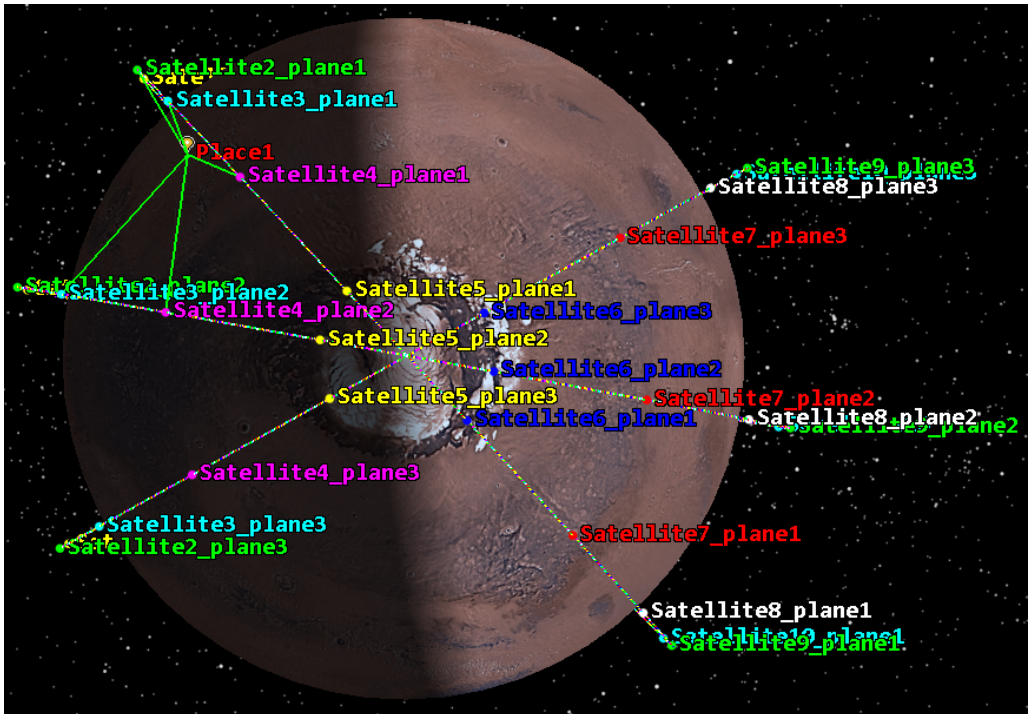

Figure 5.1 – Constellation system over Mars, N_P = 18, 3 planes.

The image above shows that this constellation is only useful if the mission requires coverage over a specific area during specific times of the day. The area labeled as Place1 is seen by at most six CubeSats for various durations over 24 hours. Place1 is not seen by any CubeSats for around one hour and 40 minutes, when it passes between plane 3 and plane 1. This is because the space between the two orbits is larger than $D_{max,S}$ and $D_{max,O}$.

Other characteristics of this system are as follows:

- Transmitter bandwidth: 0.063 MHz
- Transmitter wavelength: 0.0379 m
- Receiver bandwidth: 0.002 MHz (auto-scaled)

The three-plane constellation system shown above is especially useful for follow-up missions to places such as Mars or the Moon, where certain areas are already known. Keeping all other parameters the same, five planes are more useful for complete coverage over the central body.

5.2 SECOND CONSTELLATION SYSTEM

Parameters for another three-plane constellation model are shown in Table 5.1.

Table 5.1: Second constellation parameters, N_P = 18, 3 planes.

Parameters	Values	Comments
S	20 degrees	For satellites within each plane
t_{rev}	410.3 seconds	For discontinuous coverage
λ_{max}	24.73 degrees	Assume 5° elevation angle, Coverage in swath is continuous
λ_{street}	22.73 degrees	
$D_{max,S}$	47.47 degrees	Size of swaths away from seam
$D_{max,O}$	45.5 degrees	Size of swaths near seam

Additionally, the corresponding constellation system is shown in Figure 5.2 below.

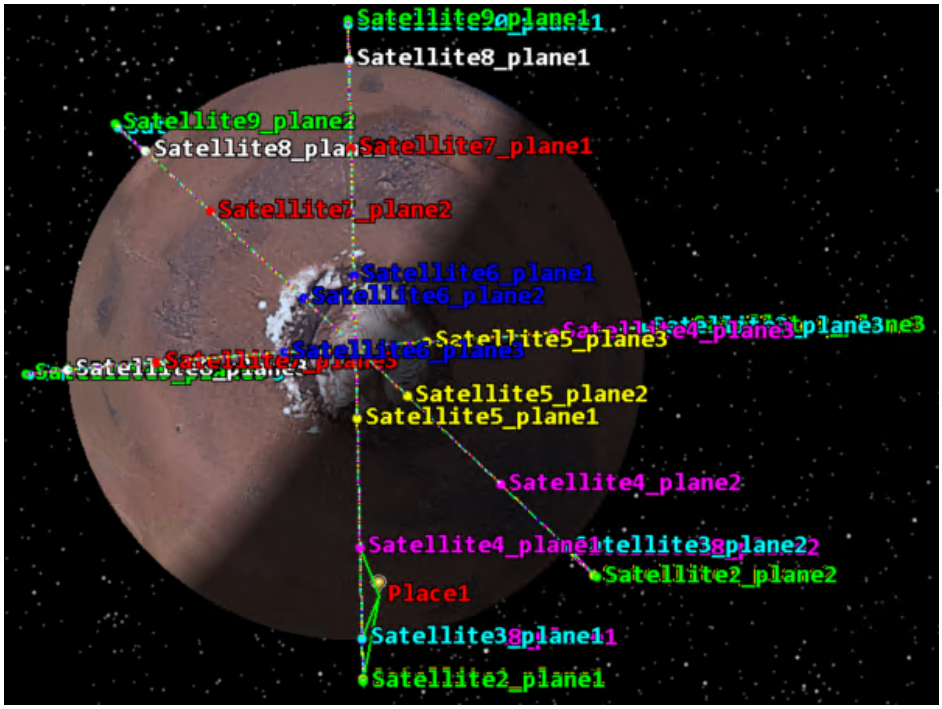

Figure 5.2 – Second constellation system over Mars, N_P = 18, 3 planes.

For this constellation, the area labeled as Place1 is seen by at most seven satellites for various durations over a 24-hour period. Place1 is not seen by any CubeSats for about 25 minutes, when it passes between plane 3 and plane 1. This period of time is far less than that of the previous constellation system due to larger swath size, which is in turn due to the lower elevation angle.

Lower elevation angles helps with using a lower number of planes to cover a lot of area. Still, keeping all other parameters the same for this system, one additional plane is needed for complete coverage over the central body.

The transmitter and receiver characteristics are the same as those of the sample constellation system, since the inputs for those instruments stayed the same.

5.3 THIRD CONSTELLATION SYSTEM

Parameters for the third three-plane constellation are shown in Table 5.2.

Table 5.2: Third constellation parameters, N_P = 18, 3 planes.

Parameters	Values	Comments
S	20 degrees	For satellites within each plane
t_{rev}	410.3 seconds	For discontinuous coverage
λ_{max}	28.36 degrees	Assume 1° elevation angle, Coverage in swath is continuous
λ_{street}	26.68 degrees	
$D_{max,S}$	55.04 degrees	Size of swaths away from seam
$D_{max,O}$	53.36 degrees	Size of swaths near seam

The corresponding constellation system is shown in Figure 5.3 below.

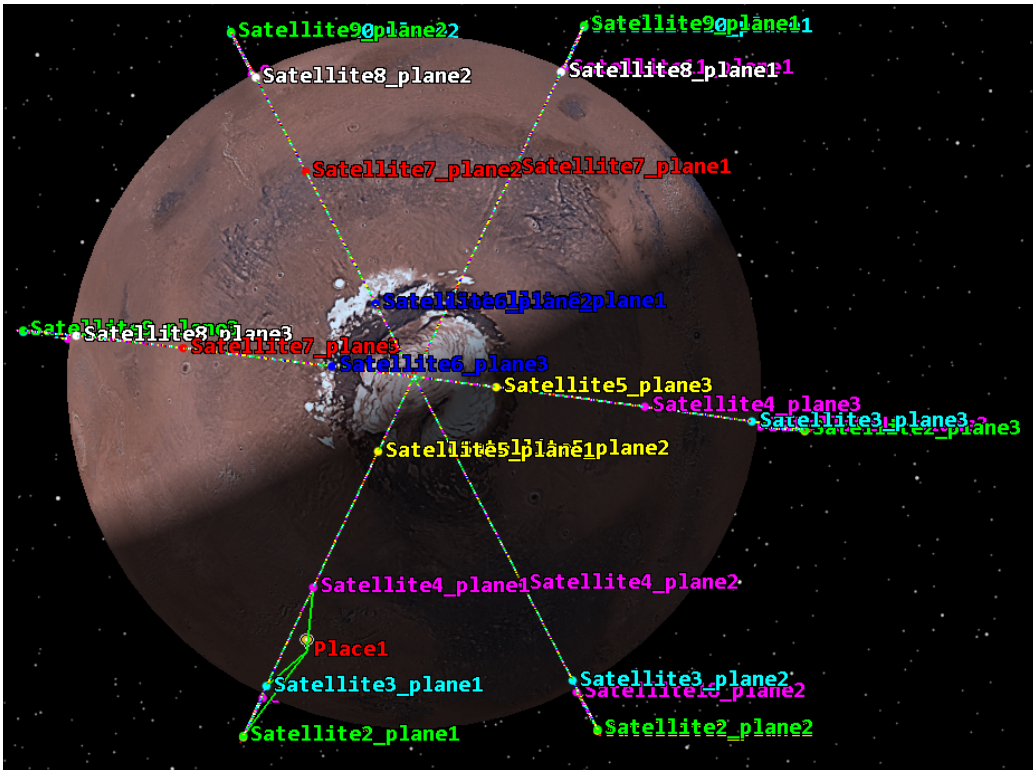

Figure 5.3 – Third constellation system over Mars, N_P = 18, 3 planes.

For this constellation, the area labeled as Place 1 is seen by at least one CubeSat throughout the entire 24-hour duration. Therefore, this constellation system can be considered as fully continuous. The transmitter and receiver characteristics are the same as those of the previous two constellation systems.

5.4 DISCUSSION

As mentioned in Section 3.3, constellations with only one or two planes are better responsive to user needs. However, for this project, three to five planes were considered to achieve better

coverage of the central body. Of the three constellation systems presented in this chapter, the third one requires the fewest number of planes to cover the most possible area. Therefore, it is the most ideal system, provided that there are no restrictions on the elevation angle.

For communications satellites, the elevation angle should be at least 5 degrees [16]. In this case, a version of the second constellation system would be the most ideal, which would have four planes instead of three to achieve maximum possible coverage. A version of the sample constellation system, with five planes instead of three, would also work; however, it would not be as ideal because it is less responsive to user needs.

The results from this chapter only correspond to an altitude of 500 km over Mars. If the central body was a larger planet such as Venus, for example, the constellation system would require more planes to cover the entire area. A smaller body such as the Moon would require no more than two planes regardless of the elevation angle.

If the altitude was decreased over Mars, more planes would be needed since the CubeSats would cover a smaller portion than before. The opposite is true if the altitude was increased, since the CubeSats would cover more area.

CONCLUSION

Constellation systems depend on user needs and specific mission requirements, as well as the type of CubeSats used. Given the calculations and simulations presented in this paper, the number of planes and CubeSats in the constellation system depend on the central body and orbit characteristics. Larger bodies generally need more planes for complete coverage, as do constellation systems with smaller orbits.

The CubeSats themselves also depend on the user needs and mission requirements, which determine the type of instruments carried. Deep space CubeSats need to communicate with ground stations on Earth, so their communication instruments should allow them to transmit and receive data over long distances. They have different power requirements than those surrounding the Earth, and the size of the CubeSat box should be able to support the total mass of all the instruments. The payload depends on the mission. For this project, the payload includes an imager/camera, altimeter, and radiometer.

A deep space CubeSat constellation system, such as those simulated in this project, provides coverage over large areas of a central body. Therefore, it would help gather data for future deep space missions. Using Mars as the central body for the simulations presented, the potential constellation systems could help determine where future missions could focus on exploring. Perhaps, these constellation systems can help determine the best areas for humans to physically explore next.

REFERENCES

[1] Klesh, A. T., and Castillo-Rogez, J. C. "Nano-Satellite Secondary Spacecraft on Deep Space Missions." *Proceedings of the Global Exploration Conference 2012*, Washington, DC, 2012.

[2] Ulybyshev, Y. "Satellite Constellation Design for Complex Coverage." *Journal of Spacecraft and Rockets*, Vol. 45, No. 4, 2008, pp. 843–849. https://doi.org/10.2514/1.35369.

[3] Wong, Y. F., Kegege, O., Schaire, S. H., Bussey, G., and Altunc, S. "An Optimum Space-to-Ground Communication Concept for CubeSat Platform Utilizing NASA Space Network and Near Earth Network." *Proceedings of the AIAA/USU Conference on Small Satellites*, 2016.

[4] Singh, L. A., Whittecar, W. R., DiPrinzio, M. D., Herman, J. D., Ferringer, M. P., and Reed, P. M. "Low Cost Satellite Constellations for Nearly Continuous Global Coverage." *Nature Communications*, Vol. 11, No. 1, 2020, pp. 1–7. https://doi.org/10.1038/s41467-019-13865-0.

[5] What Are SmallSats and CubeSats? *NASA*. 2015. https://www.nasa.gov/content/what-are-smallsats-and-cubesats. Accessed Aug. 19, 2020.

[6] Small Spacecraft, Big Universe: Lockheed Martin Selected For The Next Phase Of A Small Spacecraft Mission. *Lockheed Martin*. 2019. https://news.lockheedmartin.com/2019-06-19-Small-Spacecraft-Big-Universe-Lockheed-Martin-Selected-for-the-Next-Phase-of-a-Small-Spacecraft-Mission. Accessed Aug. 19, 2020.

[7] Hunter, R., and Korsmeyer, D. "A Review of NASA Ames CubeSat Program." *Proceedings of the Satellite Conference & Exhibition and the Hosted Payload and Smallsat Summit*, Washington, DC, 2015, pp. 1–37.

[8] Nieto-Peroy, C., and Emami, M. R. "CubeSat Mission: From Design to Operation." *Applied Sciences (Switzerland)*, Vol. 9, No. 15, 2019, pp. 1–24. https://doi.org/10.3390/app9153110.

[9] Scharf, C. A. Interplanetary CubeSats Are Go! *Scientific American*. 2019. https://blogs.scientificamerican.com/life-unbounded/interplanetary-cubesats-are-go/. Accessed Sep. 3, 2020.

[10] MarCO (Mars Cube One). *NASA*. 2019. https://solarsystem.nasa.gov/missions/mars-cube-one/in-depth/. Accessed Sep. 3, 2020.

[11] Carlisle, C., and Webb, E. H. "Space Technology 5 - A Successful Micro-Satellite Constellation Mission." *Proceedings of the AIAA/USU Conference on Small Satellites*, 2007.

[12] Braun, S., Velden, C., Greenwald, T., Herndon, D., Bennartz, R., DeMaria, M., Chirokova, G., Atlas, R. M., Dunion, J., Marks, F., Rogers, R., Christophersen, H., Annane, B., Zavodsky, B. T., and Blackwell, W. J. "Overview of the NASA TROPICS CubeSat Constellation Mission." *Proceedings of SPIE*, Vol. 10769, No. 8, 2018. https://doi.org/10.1117/12.2320333.

[13] Time-Resolved Observations of Precipitation Structure and Storm Intensity with a Constellation of Smallsats. *MIT Lincoln Laboratory*. 2019. https://tropics.ll.mit.edu/CMS/tropics/pdf/nasaTropicsFactSheet.pdf. Accessed Sep. 17, 2020.

[14] Mandl, D., Crum, G., Ly, V., Handy, M., Huemmrich, K. F., Ong, L., Holt, B., and Maharaja, R. "Hyperspectral Cubesat Constellation for Natural Hazard Response (Follow-On)." *Proceedings of the AIAA/USU Conference on Small Satellites*, 2015.

[15] Sarno, S., Graziano, M. D., and D'Errico, M. "Polar Constellations Design for Discontinuous Coverage." *Acta Astronautica*, Vol. 127, 2016, pp. 367–374. https://doi.org/10.1016/j.actaastro.2016.06.001.

[16] Larson, W. J., and Wertz, J. R. *Space Mission Analysis and Design*. Microcosm, Inc., El Segundo, CA, 1999.

[17] Anis, A. Cold Gas Propulsion System - An Ideal Choice for Remote Sensing Small Satellites. In *Remote Sensing - Advanced Techniques and Platforms* (B. Escalante, ed.), InTech, 2012, pp. 447–462.

[18] Curtis, H. *Orbital Mechanics for Engineering Students*. Elsevier, Oxford, UK, 2014.

[19] Basic Concepts of Manned Spacecraft Design: Describing Orbits. *FAA Civil Aerospace Medical Institute Library: Advanced Aerospace Medicine Online*. 154–163. https://www.faa.gov/about/office_org/headquarters_offices/avs/offices/aam/cami/library/online_libraries/aerospace_medicine/tutorial/media/III.4.1.4_Describing_Orbits.pdf. Accessed Nov. 27, 2020.

[20] Hu, Y. F., Maral, G., and Ferro, E. Appendix A: Satellite Constellation Design for Network Interconnection Using Non-Geo Satellites. In *Service Efficient Network Interconnection via Satellite*, John Wiley & Sons Ltd., New York, 2002, pp. 215–230.

APPENDIX A: ADDITIONAL EQUATIONS

A.1 ORBITAL MECHANICS CONCEPTS

Each two-body system has two frames:

- the inertial reference frame E
- the orbital frame P

To change a vector from the P frame to the E frame, a rotational matrix such as the one in Equation A.1 is used.

$$l^{E\to P} = \begin{bmatrix} cos(\Omega)cos(\omega) - sin(\Omega)cos(i)sin(\omega) & -cos(\Omega)sin(\omega) - sin(\Omega)cos(i)cos(\omega) & sin(\Omega)\,sin\,(i) \\ sin(\Omega)cos(\omega) + cos(\Omega)cos(i)sin(\omega) & -sin(\Omega)sin(\omega) + cos(\Omega)cos(i)cos(\omega) & -cos(\Omega)\,sin(i) \\ sin(i)\,sin\,(\omega) & sin(i)\,cos\,(\omega) & cos\,(i) \end{bmatrix} \quad (A.1)$$

Inputs: Ω = right ascension of the ascending node,
ω = argument of perigee,
i = inclination angle

Output: $l^{\text{E-P}}$ = rotational matrix for an ellipse

Note that the rotational matrix above is used only for elliptical orbits, for eccentricity greater than zero.

Both the radius of each CubeSat's orbit and its velocity can be expressed as vectors in the inertial reference frame using the model shown in Equation A.2.

$$\boldsymbol{X^{QE}} = l^{E\to P}\boldsymbol{X^{QP}} \quad (A.2)$$

Inputs: $l^{\text{E-P}}$ = rotational matrix for an ellipse,
$\mathbf{X^{QP}}$ = vector modeled as $x_x\mathbf{p_x} + x_y\mathbf{p_y} + x_z\mathbf{p_z}$

Output: $\mathbf{X^{QE}}$ = vector modeled as $x_x\mathbf{e_x} + x_y\mathbf{e_y} + x_z\mathbf{e_z}$

The angular momentum vector can be found using Equation A.3.

$$\boldsymbol{h} = \boldsymbol{r} \times \boldsymbol{v} \quad (A.3)$$

Inputs: **r** = radius vector modeled as $r_x\mathbf{e_x} + r_y\mathbf{e_y} + r_z\mathbf{e_z}$,
v = velocity vector modeled as $v_x\mathbf{e_x} + v_y\mathbf{e_y} + v_z\mathbf{e_z}$

Output: **h** = angular momentum vector modeled as $h_x\mathbf{e_x} + h_y\mathbf{e_y} + h_z\mathbf{e_z}$

Both inputs are vectors, so the angular momentum vector is obtained by taking the cross product. Using the angular momentum vector, Equation A.4 can be used to find the Line of Nodes.

$$\boldsymbol{n} = \boldsymbol{e_z} \times \boldsymbol{h} \quad (A.4)$$

Inputs: $\mathbf{e_z}$ = unit z-vector pointing to the north pole of the planet or moon,
h = angular momentum vector modeled as $h_x\mathbf{e_x} + h_y\mathbf{e_y} + h_z\mathbf{e_z}$

Output: **n** = Line of Nodes modeled as $-h_y\mathbf{e_x} + h_x\mathbf{e_y}$

Both inputs are vectors, so the Line of Nodes is obtained by taking the cross product. The magnitude of the Line of Nodes is used in Equation 3.8 to find the right ascension of the ascending node.

The velocity of the satellite used to find the scalar angular momentum in Equation 3.6 can be found using Equation A.5 [18].

$$v_{Satellite} = \sqrt{\frac{GM}{a}} \tag{A.5}$$

Inputs: G = gravitational constant, 6.67 x 10^{-20} $km^3/kg\text{-}s^2$,
M = mass of the planet or moon,
a = length of semi-major axis

Output: $v_{Satellite}$ = velocity of the satellite

A.2 ANGLES

The constellation structure depends on the relationship between the orbit and the central body, which is measured through angles such as the angular radius, maximum sensor look angle, and minimum elevation angle. Of the three, the minimum elevation angle is a design parameter that depends on the CubeSats used and the mission.

The angular radius, calculated using Equation A.6, is used to find several parameters of various subsystems and other calculations.

$$\rho = sin^{-1}\left(\frac{r}{a}\right) \tag{A.6}$$

Inputs: r = radius of the planet or moon,
a = length of semi-major axis

Output: ρ = angular radius of the planet or moon

The maximum sensor look angle, shown in Equation A.7, is useful for payload and orbital mechanics calculations.

$$sin(\eta_{max}) = sin(\rho) \times cos(\varepsilon_{min}) \tag{A.7}$$

Inputs: ρ = angular radius of the planet or moon,
ε_{min} = minimum elevation angle

Output: η_{max} = maximum sensor look angle

The maximum central angle used to find swath parameters shown in Section 3.3 can be calculated using Equation A.8.

$$\lambda_{max} = 90 - \varepsilon_{min} - \eta_{max} \tag{A.8}$$

Inputs: ε_{min} = minimum elevation angle,
η_{max} = maximum sensor look angle

Output: λ_{max} = maximum central angle

A.3 TORQUES

The worst-case disturbance torque is made up of four components: maximum gravity torque, solar radiation torque, magnetic torque, and aerodynamic torque. The values for each of the torque values depend on the central body considered for the mission, as well as the size of the CubeSat.

The maximum gravity torque is calculated using Equation A.9. This parameter has the most impact if the orbit altitude is small and the mass of the central body is large; in other words, it is useful if the central body has a gravity field.

$$T_G = \frac{3GM}{2a^3}\left|I_z - I_y\right| sin(2\theta) \qquad (A.9)$$

Inputs: G = gravitational constant, 6.67 x 10^{-20} $km^3/kg\text{-}s^2$,
M = mass of the planet or moon,
a = length of semi-major axis,
I_z = moment of inertia about z,
I_y = moment of inertia about y,
θ = maximum deviation of the z-axis from local vertical

Output: T_G = maximum gravity torque

The solar radiation torque is calculated using Equation A.10. This parameter depends on the amount of sunlight in contact with the CubeSats. For the sample calculations in this project, the solar radiation torque had the most impact on the disturbance torque, possibly because of the distance from the sun.

$$T_{sp} = \frac{F_s A}{c}\left(c_{ps} - cg\right)(1+q)\, cos(I) \qquad (A.10)$$

Inputs: F_s = solar constant,
A = CubeSat surface area,
c = speed of light, 3.00 x 10^8 m/s,
c_{ps} = location of center of solar pressure,
cg = center of gravity,
q = reflectance factor,
I = angle of incidence of the Sun

Output: T_{sp} = solar radiation torque

The magnetic torque is calculated using Equation A.11. Usually, this parameter is useful for central bodies with a high magnetic field such as the Earth. It is not useful for central bodies like the Moon or Mars.

$$T_m = DB \qquad (A.11)$$

Inputs: D = residual dipole,
B = magnetic field

Output: T_m = magnetic torque

The aerodynamic torque is calculated using Equation A.12. This parameter is only useful if the central body has an atmosphere.

$$T_a = \frac{1}{2}\rho A c_D v_{satellite}^2 (c_{pa} - cg) \qquad (A.12)$$

Inputs: ρ = atmospheric density,
A = CubeSat surface area,
c_D = coefficient of drag,
$v_{satellite}$ = velocity of the satellite,
c_{pa} = center of aerodynamic pressure,
cg = center of gravity

Output: T_a = aerodynamic torque

APPENDIX B: SAMPLE CALCULATIONS

This section includes the Microsoft Excel tables for all three simulations shown in this paper, as well as other calculations and values. The constellation system calculations are shown in the first three sections. Subsystem calculations are shown in other sections.

B.1 SIMULATION ONE

Table B.1: Input parameters for simulation 1.

Parameters	**Values**
Number of satellites (N)	18 satellites
Space between satellites (S)	20 degrees
Numbers of planes (p)	3 planes
Revisit time (t_{rev})	410.3366 seconds

Table B.2: Angle parameters for simulation 1.

Parameters	**Values (radians)**	**Values (degrees)**
Min elevation angle (ε_{min})	0.174533	10
Angular radius (ρ)	1.058599	60.65327
Max sensor look angle (η_{max})	1.032196	59.14045
Max central angle (λ_{max})	0.364068	20.85955
Street of coverage angle (λ_{street})	0.321155	18.40081
Max separation, same direction ($D_{max,S}$)	0.685223	39.26036
Max separation, opposite direction ($D_{max,O}$)	0.642309	36.80162

Table B.3: Right ascensions of the ascending node per plane for simulation 1.

Plane	**Ω (degrees)**
1	0
2	36.80162
3	76.06198
4	115.3223
5	152.124

Table B.4: Arguments of latitude per satellite in each plane for simulation 1.

Satellite	1	2	3	4	5	6	7	8	9
u (degrees)	0	20	40	60	80	100	120	140	160
Satellite	10	11	12	13	14	15	16	17	18
u (degrees)	180	200	220	240	260	280	300	320	340

B.2 SIMULATION TWO

Input parameters are the same as shown in Table B.1. Other parameters, shown below, differ from simulation 1 because the minimum elevation angle is different.

Table B.5: Angle parameters for simulation 2.

Parameters	Values (radians)	Values (degrees)
Min elevation angle (ε_{min})	0.087266	5
Angular radius (ρ)	1.058599	60.65327
Maximum sensor look angle (η_{max})	1.051871	60.26779
Maximum central angle (λ_{max})	0.431658	24.73221
Street of coverage angle (λ_{street})	0.396846	22.73759
Max separation, same direction ($D_{max,S}$)	0.828504	47.4698
Max separation, opposite direction ($D_{max,O}$)	0.793692	45.47518

Table B.6: Right ascensions of the ascending node per plane for simulation 2.

Plane	Ω (degrees)
1	0
2	45.47518
3	92.94498
4	140.4148
5	185.89

Plane 5 is not considered for the constellation system because of its high Ω angle. If added into the system, the plane would cut into another swath.

The arguments of latitude are the same as in simulation 1 because the N and S values are the same as in simulation 1.

B.3 SIMULATION THREE

Input parameters are the same as shown in Table B.1. Other parameters are different because the minimum elevation angle is different.

Table B.7: Angle parameters for simulation 3.

Parameters	Values (radians)	Values (degrees)
Min elevation angle (ε_{min})	0.017453	1
Angular radius (ρ)	1.058599	60.65327
Maximum sensor look angle (η_{max})	1.058328	60.63775
Maximum central angle (λ_{max})	0.495015	28.36225
Street of coverage angle (λ_{street})	0.465635	26.67893
Max separation, same direction ($D_{max,S}$)	0.96065	55.04117
Max separation, opposite direction ($D_{max,O}$)	0.93127	53.35785

Table B.8: Right ascensions of the ascending node per plane for simulation 3.

Plane	Ω (degrees)
1	0
2	53.35785
3	108.399
4	163.4402
5	216.7981

Planes 4 and 5 are not considered for the constellation system because of their high Ω angle. If added into the system, the two planes would interfere with coverage from other CubeSats.

Like in simulation 2, the arguments of latitude are the same as in simulation 1, since there is no change in the N and S values.

B.4 POWER SUBSYSTEM CALCULATIONS

Table B.9: Sample parameters of the solar arrays.

Parameter	Value
Power requirement, eclipse (P_e)	14 W
Power requirement, daylight (P_d)	14 W
Period length, eclipse (T_e)	7386.059 s
Period length, daylight (T_d)	7325.406 s
Transmission efficiency, eclipse (X_e)	0.6
Transmission efficiency, daylight (X_d)	0.8
Power needed from solar array (P_{sa})	41.02653 W
Solar flux	590
Efficiency	0.185
Ideal solar cell performance (P_O)	109.15 W
Inherent degradation (I_d)	0.77
Sun incidence angle (θ)	23.5 degrees
Beginning-of-life power/area (P_{BOL})	77.07477 W
degradation	0.275
Satellite life	3 years
Life degradation of solar array (L_d)	0.381078
End-of-life power/area (P_{EOL})	29.37151 W

Table B.10: Sample parameters of batteries.

Parameter	Value
Eclipse duration (τ_e)	7386.059 s
Depth of discharge (DOD)	0.9
Number of batteries (N)	2

Transmission efficiency (n)	300
Required battery capacity (C_r)	191.4904 W-hr
Specific energy density	265
Mass of batteries	0.722605

B.5 COMMUNICATIONS SUBSYSTEM CALCULATIONS

Table B.11: Sample data parameters for communications.

Parameter	**Value**
Data rate (DR)	32327.4343 bps
Fractional reduction (F)	0.77
Max time in view (Tmax)	3600 s
Initiation time (Tinitiate)	120 s
Margin accounting for missed passes	3
Quantity of data (DQ)	28577452 bits

Table B.12: Transmitter parameters for communications.

Parameter	**Value**
Power flux density (W_f)	-142 dBW/m^2
Path length (S)	0.48 m
Frequency (f)	7.90E+09 Hz
Effective isotropic radiated power (EIRP)	2855.0794 dB
Space loss (L_s)	-44.019139 dB
Path loss (L_a)	-0.3 dB
Receive antenna gain (G_r)	40 dBi
Noise temperature (T_s)	614 K
Received energy/bit to noise density (E_b/N_o)	2.17E+02 dB
Antenna diameter (D)	0.001 m
antenna half-power beamwidth (θ)	0.000152 degrees
Pointing error (e)	0.0001
Antenna pointing loss (L_θ)	-16982.313 dB

Table B.13: Receiver parameters for communications.

Parameter	**Value**
Power flux density (W_f)	-142 dBW/m^2
Path length (S)	0.48 m
Frequency (f)	7.25E+09 Hz
Effective isotropic radiated power (EIRP)	2855.0794 dB
Space loss (L_s)	-43.273357 dB

Path loss (L_a)	-0.3 dB
Receive antenna gain (G_r)	40 dBi
Noise temperature (T_s)	135 K
Received energy/bit to noise density (E_b/N_o)	2.24E+02 dB
Antenna diameter (D)	0.001 m
antenna half-power beamwidth (θ)	0.000166 degrees
Pointing error (e)	0.0001
Antenna pointing loss (L_θ)	-14302.721 dB

B.6 GN&C SUBSYSTEM CALCULATIONS

Both types of torque are in separate tables shown below.

Table B.14: Parameters relating to disturbance rejection.

Parameter	**Value**
Mass of the planet/moon (M)	6.42E+23 kg
Orbit radius (a)	3896.2 km
Max deviation of z-axis from local vertical (θ)	30 degrees
Moment of inertia about z (I_z)	1.66667E-05 m^4
Moment of inertia about y (I_y)	6.66667E-05 m^4
Maximum gravity torque (T_G)	4.70E-20 N-m
CubeSat surface area (A)	0.02 m^2
Solar constant (F_s)	1370
Reflectance factor (q)	0.6
Angle of incidence of Sun (I)	0
Location of center of solar pressure (c_{ps})	0.005 m
Center of gravity (cg)	0.01 m
Solar radiation torque (T_{sp})	-7.31E-10 N-m
Residual dipole (D)	1
Magnetic field (B)	0
Magnetic torque (T_m)	0
Atmospheric density (ρ)	1.00E-09 kg/m^3
Coefficient of drag (c_D)	2
Spacecraft velocity ($v_{satellite}$)	3.314425912 km/s
Center of aerodynamic pressure (c_{pa})	0.015 m
Aerodynamic torque (T_a)	1.09854E-06 N-m
Worst-case disturbance torque (T_D)	1.09781E-06 N-m
Margin factor (MF)	1
Reaction wheel torque due to disturbance rejection (T_{RW})	1.09781E-06 N-m

Orbit period (τ)	7386.059379 s
Wheel momentum (h)	0.001433394 N-m-s

Table B.15: Parameters relating to slew torque.

Parameter	**Value**
Slewing angle (θ)	30 degrees
CubeSat moment of inertia (I)	1.66667E-05 m^4
Minimum maneuver time (t)	5 seconds
Slew torque (T_{slew})	1.39626E-06 N-m

B.7 PROPULSION SUBSYSTEM CALCULATIONS

Table B.16: Parameters for the cold gas thruster.

Parameter	**Value**
specific heat ratio (gamma)	1.32
molecular weight of gas (MW)	0.017 kg/mol
chamber temperature (T_c)	300 K
exit pressure (P_e)	40000 Pa
chamber pressure (P_c)	800000 Pa
exhaust velocity (V_e)	790.512204 m/s
mass flow rate ($\dot{m}$)	-2.529942 kg/s
exit area (A_e)	0.05 m^2
throat area (A_t)	0.001 m^2
expansion ratio (ε)	50
Thrust (F)	0.05 N
Specific Impulse (I_{sp})	50 s
characteristic velocity (c*)	-316.21279 m/s
thrust coefficient (c_F)	0.16666667

B.8 STRUCTURES SUBSYSTEM CALCULATIONS

These material properties were not listed in the List of Symbols, but they were used for calculating CubeSat box parameters. The box parameters are shown in the next table.

Table B.17: Additional material properties for Al 7075-T73.

Material Property	**Value**
Ultimate factor of safety (FS_u)	1.25
Yield factor of safety (FS_y)	1.1
Load factor, axial	6.5
Load factor, lateral	3

Table B.18: Parameters for the CubeSat box.

Parameter	Value
cross-sectional area (A)	0.02 m^2
distributed mass (m_B)	25 kg
Area moment of inertia (I_z)	1.66667E-05 m^4
Area moment of inertia (I_y)	6.66667E-05 m^4
axial frequency ($f_{nat,a}$)	3.44E+03 Hz
lateral frequency ($f_{nat,l}$)	7.41E+02 Hz
moment arm (y)	0.15 m
bending moment (M)	36.8 N-m
limit load (P_{eq})	2.33E+03 N
ultimate eq axial load ($P_{eq,u}$)	2.91E+03 N
yield eq axial load ($P_{eq,y}$)	2.56E+03 N
critical buckling load (P_{cr})	3.24E+07 N
margin of safety (MS)	1.11E+04
mass of box shell (m_{box})	16.8 kg

Both the gas tank and solar array parameters are shown in separate tables. No specific material was considered for the gas tank.

Table B.19: Sample parameters of the thruster's gas tank.

Parameter	Value
Max expected operating pressure (P)	1.00E+07 Pa
Radius	0.03 m
Thickness	0.004 m
Allowable stress (spherical)	37500000 Pa
Allowable stress (cylindrical)	75000000 Pa

Table B.20: Sample parameters of the solar array.

Parameter	Value
Power needed from solar array, daylight (P_{sa})	41.02652985 W
End-of-life power/area (P_{EOL})	29.37150978 W
Required solar array area (A_{sa})	1.396813788 m^2
Mass of solar arrays (m_a)	1.641061194 kg

The total mass of the CubeSat is based on the material used in some of the components, such as the CubeSat box and solar arrays. For other components (i.e. wheels and gas tank), estimates were used based on existing models. The propellant mass depends on the propellant used for calculating values in Table B.16.

Table B.21: Sample masses of CubeSat components.

Component	Mass (kg)
Total batteries	1.44521078
Wheels	1
Propellant (NH3)	0.0184302
CubeSat box, shell	16.8
Solar arrays	1.64106119
Gas tank	2
Total	22.9047022

B.9 PAYLOAD SUBSYSTEM CALCULATIONS

Table B.22: Parameters for payload data.

Parameter	Value
Max along-track ground sampling distance (Y_{max})	50 m
Slant range (R_s)	1200 m
Instantaneous field of view (IFOV)	2.38732415
Number of cross-track pixels (Z_C)	25.399882 pixels
Number of swaths in one second (Z_A)	159.092444 swath/s
Number of bits per pixel (B)	8 bits
Data rate (DR)	32327.4343 bps